© 2018. Published by The Company of Biologists Ltd | Development (2018) 145, dev161398. doi:10.1242/dev.161398

RESEARCH ARTICLE

ANGUSTIFOLIA contributes to the regulation of three-dimensional morphogenesis in the liverwort *Marchantia polymorpha*

Tomoyuki Furuya[1], Koro Hattori[1], Yoshitaka Kimori[2,*], Sakiko Ishida[3], Ryuichi Nishihama[3], Takayuki Kohchi[3] and Hirokazu Tsukaya[1,4,‡]

ABSTRACT

Arabidopsis thaliana mutants deficient in ANGUSTIFOLIA (AN) exhibit several phenotypes at the sporophyte stage, such as narrow and thicker leaves, trichomes with two branches, and twisted fruits. It is thought that these phenotypes are caused by abnormal arrangement of cortical microtubules (MTs). AN homologs are present in the genomes of diverse land plants, including the basal land plant *Marchantia polymorpha*, and their molecular functions have been shown to be evolutionarily conserved in terms of the ability to complement the *A. thaliana an-1* mutation. However, the roles of ANs in bryophytes, the life cycle of which includes a dominant haploid gametophyte generation, remain unknown. Here, we have examined the roles of AN homologs in the model bryophyte *M. polymorpha* (MpAN). Mp*an* knockout mutants showed abnormal twisted thalli and suppressed thallus growth along the growth axis. Under weak blue light conditions, elongated thallus growth was observed in wild-type plants, whereas it was suppressed in the mutants. Moreover, disordered cortical MT orientations were observed. Our findings suggest that MpAN contributes to three-dimensional morphogenesis by regulating cortical MT arrangement in the gametophytes of bryophytes.

KEY WORDS: Liverwort, Gametophyte, Morphogenesis, Cell morphology, Cortical microtubules

INTRODUCTION

ANGUSTIFOLIA (AN) of *Arabidopsis thaliana* (L.) Heynh. plays important roles in morphogenesis. Deficient mutants of AN express narrow and thicker leaves, twisted fruits and petals, and premature opening of flowers (Rédei, 1962; Tsukaya et al., 1994, 1996; Bai et al., 2010, 2013). At the cellular level, *A. thaliana an* leaves show reduced cell width expansion and enhanced cell thickness expansion in palisade tissue, a simpler epidermal cell shape and trichomes with two branches (Tsukaya et al., 1994; Hülskamp et al., 1994; Tsuge et al., 1996). It is thought that these phenotypes are caused by the abnormal arrangement of cortical MTs with altered orientation in palisade cells, which are more regularly aligned to be parallel to each other in the epidermal cells and have disrupted density gradient in the trichome cells (Kim et al., 2002; Folkers et al., 2002). A GFP-fused AN protein was distributed in a punctate manner in the cytosol, partially colocalizing with the trans-Golgi network (Minamisawa et al., 2011). In addition, AN protein is colocalized with stress granules under stress conditions, such as high temperature (Bhasin and Hülskamp, 2017). Moreover, *an* mutants show tolerance toward biotic and abiotic stresses, including pathogens, salt and osmotic stresses (Gachomo et al., 2013; Bhasin and Hülskamp, 2017). However, the molecular functions of AN in morphogenesis and stress responses are unknown. Use of a yeast two-hybrid system and pull-down assay resulted in the identification of several AN-interacting proteins; e.g. a receptor kinase STRUBBELIG/SCRAMBLED, a kinesin motor molecule ZWICHEL (ZWI), ANGUSTIFOLIA INTERACTING KINASE (AIK1) and ASYMMETRIC LEAF ENHANCER 3 (AE3), as well as several RNA-binding proteins (Folkers et al., 2002; Bai et al., 2013; Kwak et al., 2015; Bhasin and Hülskamp, 2017). Mutants of STRUBBELIG/SCRAMBLED and AN have similar phenotypes, such as twisted fruits, petals and roots, suggesting that these function cooperatively during morphogenesis [Fulton et al., 2009; Bai et al., 2013, who reported that *DETORQUEO* (*DOQ*) corresponds to *AN*; Kwak et al., 2015].

AN is widely conserved in Streptophyta, and plant ANs are homologs of animal C-terminal binding proteins (CtBPs), which function as transcriptional co-repressors (Kim et al., 2002; Folkers et al., 2002; Chinnadurai, 2007). Both CtBPs and ANs have high amino acid sequence homology to NAD(H)-dependent d-isomer-specific 2-hydroxy acid dehydrogenases (D2-HDH) (Kim et al., 2002). However, plant ANs lack the residues essential for activity of the D2-HDH motif (Kim et al., 2002; Tsukaya, 2006; Stern et al., 2007). Indeed, *A. thaliana* AN does not exhibit dehydrogenase activity and binding ability with adenovirus E1A protein, a well-known CtBP-binding protein in a dehydrogenase activity-dependent manner (Cho et al., 2008; Stern et al., 2007). Moreover, *A. thaliana* AN cannot rescue the zygotic lethal phenotype caused by loss-of-function of CtBP in the fruit fly *Drosophila melanogaster* (Stern et al., 2007). These findings suggest that plant ANs are functionally distinct from animal CtBPs. In contrast, plant ANs from the angiosperm *Ipomoea nil* (L.) Roth (Japanese morning glory), the gymnosperm *Larix gmelinii* (Dahurian larch) and the liverwort *Marchantia polymorpha* can rescue the phenotype of narrow leaves of the *A. thaliana an-1* mutant, suggesting that the molecular functions of AN in plants are evolutionarily conserved (Cho et al., 2005; Lin et al., 2008; Minamisawa et al., 2011). Based on their sequence similarity, it is

[1]Department of Biological Sciences, Graduate School of Science, University of Tokyo, Tokyo 113-0033, Japan. [2]Department of Imaging Science, Center for Novel Science Initiatives, National Institutes of Natural Sciences, Okazaki 444-8787, Japan. [3]Graduate School of Biostudies, Kyoto University, Kyoto 606-8502, Japan. [4]Okazaki Institute for Integrative Bioscience, National Institutes of Natural Sciences, Okazaki 444-8787, Japan.
*Present address: Department of Management and Information Sciences, Faculty of Environmental and Information Sciences, Fukui University of Technology, Fukui 910-8505, Japan.

‡Author for correspondence (tsukaya@bs.s.u-tokyo.ac.jp)

T.F., 0000-0002-0419-7520; R.N., 0000-0002-7032-732X; T.K., 0000-0002-9712-4872; H.T., 0000-0002-4430-4538

Received 11 November 2017; Accepted 6 August 2018

Development (2018) 145, dev161398. doi:10.1242/dev.161398

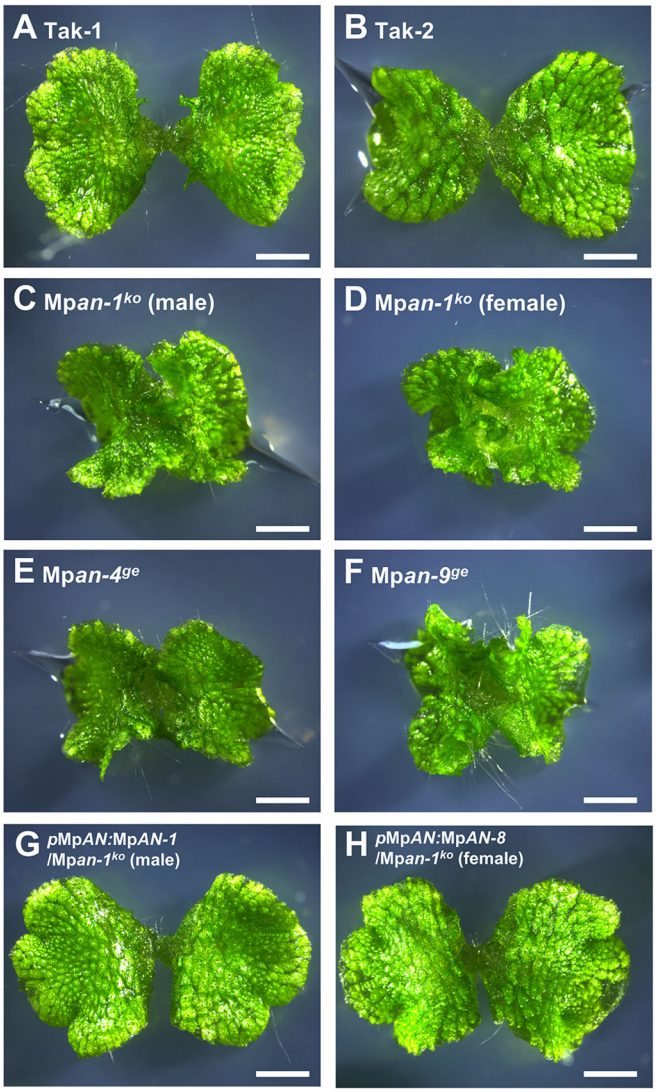

Fig. 1. Morphology of Mp*an* mutants. (A-H) 12-day-old gemmalings of the wild-type lines Tak-1 (A) and Tak-2 (B); the Mp*an* knockout lines Mp*an-1*^{ko} (male) (C) and Mp*an-1*^{ko} (female) (D); the Mp*an* genome-edited lines Mp*an-4*^{ge} (E) and Mp*an-9*^{ge} (F); and the complementation lines pMp*AN*:Mp*AN*-1/Mp*an-1*^{ko} (male) (G) and pMp*AN*:Mp*AN*-8/Mp*an-1*^{ko} (female) (H). Scale bars: 3 mm.

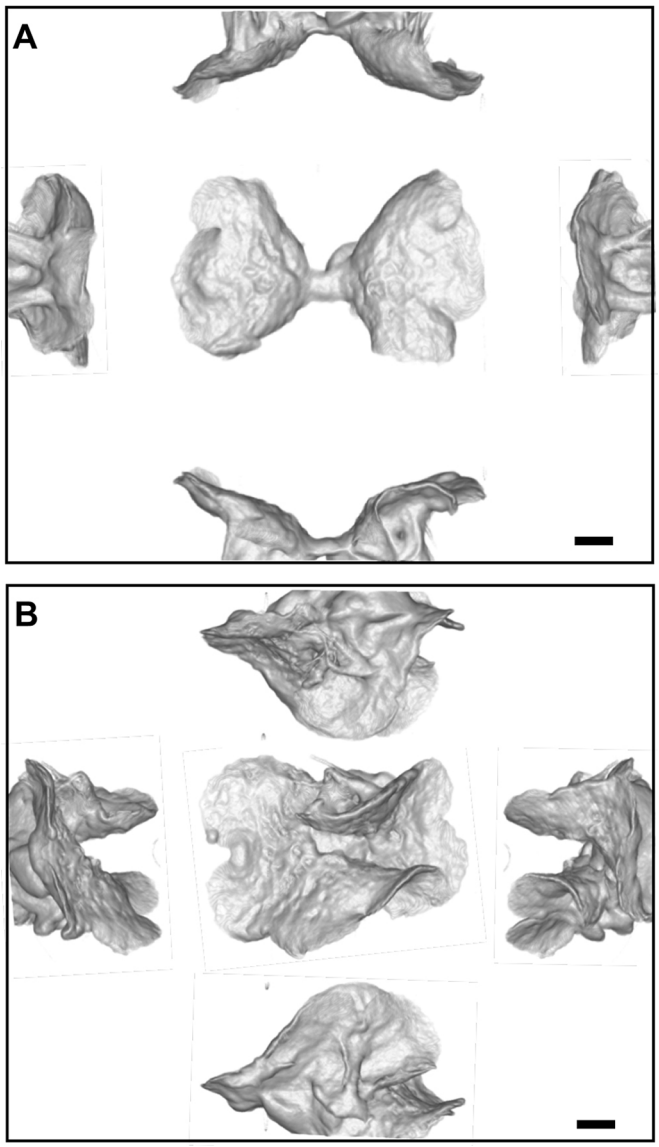

Fig. 2. Micro-CT image of an Mp*an* mutant. (A,B) Micro-CT images of 10-day-old gemmalings of Tak-1 (A) and Mp*an-1*^{ko} (male) (B). Central images show a top view; peripheral images show side views. Scale bars: 1 mm.

thought that animal CtBPs and plant ANs evolved from the NAD(H)-dependent D-hydroxyacid dehydrogenase (Stern et al., 2007). After divergence of animals and plants, the ancestral plant AN lost its dehydrogenase activity due to a deficient D2-HDH motif and the ancestral animal CtBP acquired the PLDLS-binding motif and RRT-binding motif required for co-repressor activity (Stern et al., 2007).

Liverworts, together with mosses and hornworts, make up the basal land-plant lineage bryophytes (Wickett et al., 2014). The liverwort *M. polymorpha* is used as a model plant because of its short life cycle, easy culture and crossing, lower level of genetic redundancy, and the availability of genetic information and gene manipulation systems (Ishizaki et al., 2016; Shimamura, 2016; Bowman et al., 2017). In bryophytes, the haploid gametophytic generation dominates the diploid sporophytic generation (Ishizaki, 2017). During gametophytic generation, *M. polymorpha* forms thalli as the main vegetative plant body. Thalli grow by repeated dichotomous branching (bifurcation) of apical notches, which is the site of cell proliferation (Shimamura, 2016; Solly et al., 2017). *M. polymorpha* can propagate not only by sexual reproduction via spore formation but also by asexual reproduction via gemma formation in the gemma cup on the thallus (Shimamura, 2016). As described above, the AN homolog from *M. polymorpha* (MpAN) can rescue the *an-1* mutation of *A. thaliana* (Minamisawa et al., 2011). However, previous analyses of the roles and molecular functions of plant ANs were limited to the diploid sporophyte phase; no phenotype has been recognized in the haploid gametophyte phase. Therefore, analyses of the roles of MpAN in gametophytes of *M. polymorpha* will enhance our understanding of the roles of plant ANs in land plants and the evolution thereof.

Here, we report the morphology of Mp*an* knockout mutants of *M. polymorpha*. These mutants have abnormal twisted thalli and suppressed thallus growth along the growth axis due to irregular cell expansion. Moreover, cortical MTs were disordered in Mp*an* knockout mutants. In this article, we first report the roles of MpAN as a coordinator for arrangement of cortical MTs to form the

Development (2018) 145, dev161398. doi:10.1242/dev.161398

well-ordered cell and tissue morphogenesis in gametophyte phase of *M. polymorpha* and discuss the comparison with other plant ANs.

RESULTS

Morphology of Mp*an* mutants

Mp*AN* is a broadly expressed gene in both the gametophyte phase, including gemmae, gemmalings, reproductive organs and sporelings, and the sporophyte phase, based on information available on the public database MarpolBase (marchantia.info) (Fig. S1A-C). To evaluate the roles of MpAN in *M. polymorpha*, we created Mp*an* knockout lines and Mp*an* genome-edited lines. The Mp*an* knockout lines were constructed by homologous recombination (Fig. S2A) (Ishizaki et al., 2013). Mp*an-1*^{ko} (male) and Mp*an-1*^{ko} (female) were isolated as described in the Materials and Methods section, and confirmed by genomic PCR (Fig. S2C). We also isolated Mp*an* genome-edited lines constructed using the CRISPR/Cas9 system: Mp*an-4*^{ge} (male) and Mp*an-9*^{ge} (female) (Fig. S2B,C).

In 12-day-old gemmalings, the knockout lines Mp*an-1*^{ko} (male) and Mp*an-1*^{ko} (female), and the genome-edited lines Mp*an-4*^{ge} and Mp*an-9*^{ge} showed less flattening of thalli than did the wild-type lines Takaragaike-1 (Tak-1) and Takaragaike-2 (Tak-2) (Fig. 1). To visualize thallus morphology in detail, we captured three-dimensional (3D) images by micro-computed tomography (micro-CT) (Fig. 2; Movies 1 and 2). Mp*an-1*^{ko} (male) showed an abnormal shape of the thallus, which was twisted along the growth axis. Moreover, the thallus morphology of the complementation lines *p*Mp*AN:*Mp*AN*-1/Mp*an-1*^{ko} (male) and *p*Mp*AN:*Mp*AN*-8/Mp*an-1*^{ko} (female) were restored to those of the wild-type lines, demonstrating that the abnormal thallus formation of the knockout lines was caused by loss-of-function of MpAN (Fig. 1). When using the deletion construct of the plant-specific C-terminal region in MpAN for the complementation test, the thallus phenotype of Mp*an-1*^{ko} was not rescued (Fig. S3). These results suggest that the plant-specific C-terminal region of MpAN has a role at least in thallus morphogenesis. Moreover, the same promoter region of Mp*AN* for the complementation test was used to observe the expression pattern (Fig. S1C,D). Mp*AN* was well expressed around apical notches known as active growth areas, in both *p*Mp*AN:Citrine-NLS* and *p*Mp*AN:GUS* transgenic plants.

M. polymorpha develops characteristic reproductive organs: antheridiophores and archegoniophores in males and females, respectively. The antheridiophores of Mp*an-1*^{ko} (male) showed an abnormal mushroom-like antheridial receptacle with a curled and waved margin, whereas the wild-type and complementation lines had flatter disc-like shapes (Figs S4 and S5). The archegoniophores of Mp*an-1*^{ko} (female) had thicker digitate rays compared with those of the wild-type and complementation lines (Fig. S4). Although Mp*AN* expression was detected in both antheridiophores and archegoniophores of *p*Mp*AN:GUS* transgenic plants, the GUS signal was not detected in the antheridium or archegonium, except for the younger antheridium (Fig. S1). Normal sporophytes and spores were produced following crossing of Mp*an-1*^{ko} (female) with Mp*an-1*^{ko} (male), indicating that the knockout lines have normal morphology and fertility (Fig. S6). In addition, Mp*AN* expression was not detected in the early embryo stages following crossing of *p*Mp*AN:GUS* transgenic plants (Fig. S1M).

Development of Mp*an* mutants

To examine in detail the differences between the wild-type and Mp*an* knockout lines, we traced the development of gemmalings for 10 days (Fig. 3). After day 5, the Mp*an* knockout [Mp*an-1*^{ko} (male) and Mp*an-1*^{ko} (female)] lines showed enhanced vertical twisting growth. On the other hand, the fresh weight of 10-day-old gemmalings in Tak-1 and Mp*an-1*^{ko} were 9.98±2.76 mg (n=22) and 9.39±1.34 mg (n=19), respectively, indicating no significant difference using Student's t-test (P=0.41). Next, we measured

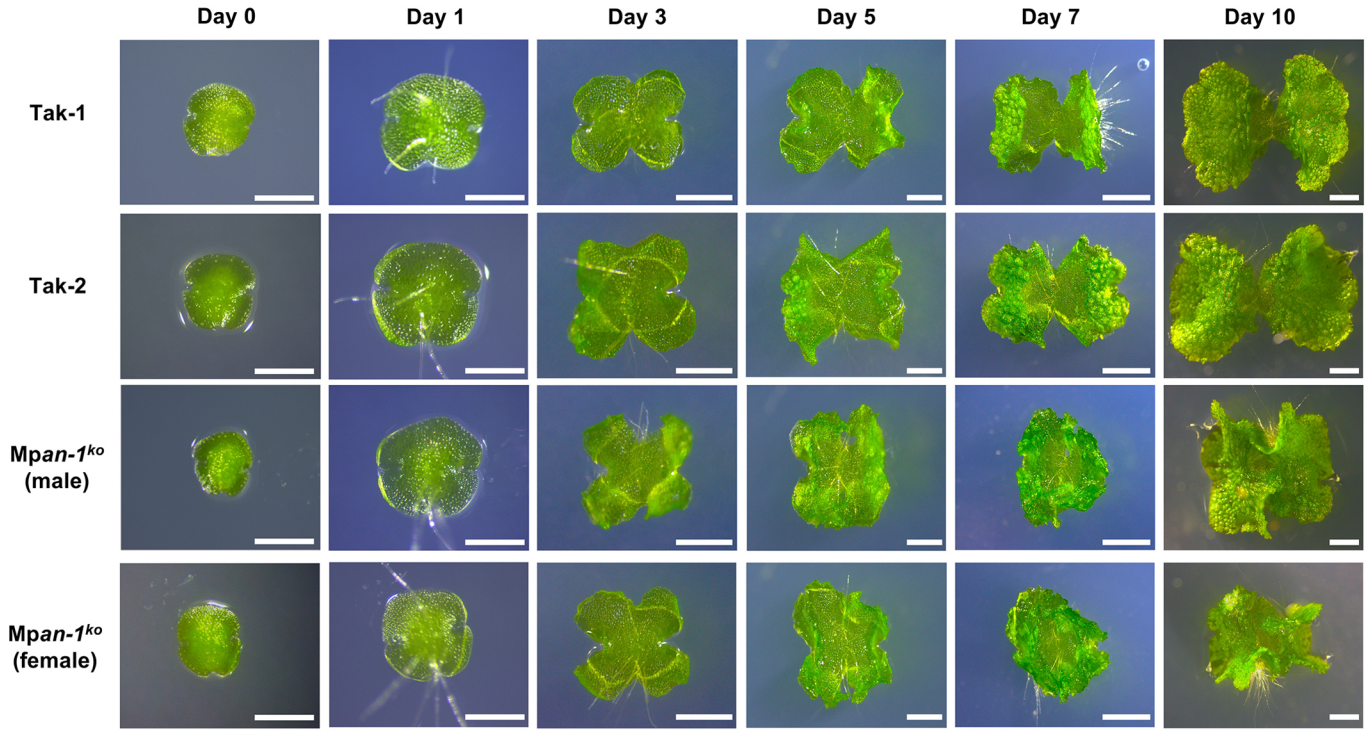

Fig. 3. Time-course observation of Mp*an* mutants. The wild-type lines Tak-1 and Tak-2, and the Mp*an* knockout lines Mp*an-1*^{ko} (male) and (female) were observed at the indicated time points during growth from the gemma. Scale bars: 0.5 mm (0 and 1 day), 1 mm (3 and 5 days) and 2 mm (7 and 10 days).

Development (2018) 145, dev161398. doi:10.1242/dev.161398

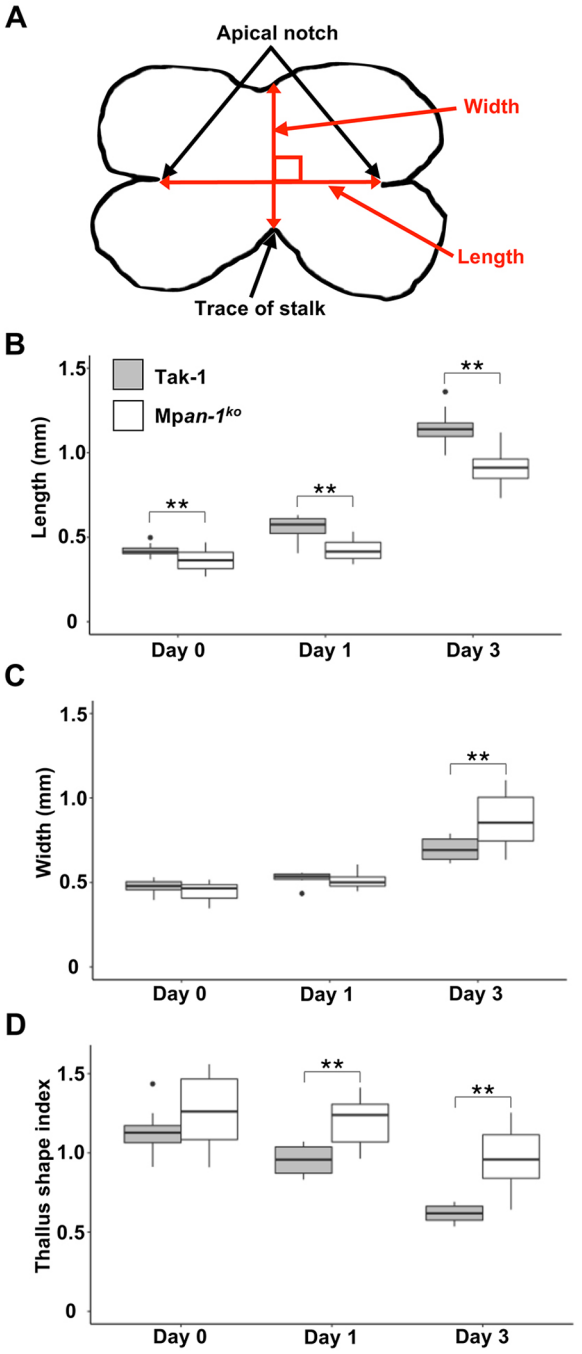

Fig. 4. Shapes of gemmae and thalli in Mp*an* mutants. (A) Evaluation schematic of the shapes of gemmae and thalli. (B-D) Length and width of gamma and thalli. The 'thallus-shape index' was calculated by width per length. Length (B), width (C) and thallus-shape index (D) values are shown in box-and-whisker plots. Median values (middle bars) and first to third interquartile ranges (boxes); whiskers indicate 1.5× the interquartile ranges; dots indicate outliers; $9 \leq n \leq 17$. $^{**}P<0.01$ compared with Tak-1; Student's *t*-test.

the shape of Tak-1 and Mp*an-1*^{ko} gemmalings visualized with the modified pseudo-Schiff propidum iodide (mPS-PI) staining. The 'length' was defined as distance between the apical notches, and the 'width' as distance from the trace of the stalk to the opposite side across the length at 90° (Fig. 4A). In addition, the gemma/thallus shape index was calculated as the ratio of the width to length. Mp*an-1*^{ko} from the gemma stage exhibited a shorter length on day 3 compared with Tak-1, resulting in a more square-shaped thallus in Mp*an-1*^{ko} than in Tak-1 (Fig. 4, Fig. S7). For longer-term observations, we cultured Tak-1 and Mp*an-1*^{ko} (male) on rockwool (Fig. S8). By day 35, Tak-1 had formed radially expanded thalli, whereas Mp*an-1*^{ko} showed an overlapped and waved form around the basal part of the thalli, which developed earlier or at the early notch plastochron stage (Solly et al., 2017), and were slightly wider and rounded around the distal growing part. Although the gross shape of the thalli of the Mp*an* knockout lines was abnormal, they formed air pores after day 5 and gemma cups at a later stage (Fig. 3, Fig. S8).

In general, the extent and location of cell proliferation are important for morphogenesis. Gemma of *M. polymorpha* have two apical notches, where cell proliferation occurs, and grow by bifurcation of the apical notches (Fig. S8A; Solly et al., 2017). However, observation of the apical notches in knockout lines was hampered by the wavy margin of their thalli. Thus, the cell proliferation region was visualized by 5-ethynyl-2′-deoxyuridine (EdU) staining (Nishihama et al., 2015; Yin and Tsukaya, 2016) (Fig. 5). The apical notches on Tak-1 and Mp*an-1*^{ko} were similar in number, location and timing of bifurcation (Fig. 5), indicating that the knockout line had the normal growth pattern of thallus.

Next, to identify the factor(s) that influence the thallus shapes of the knock-out lines, we enumerated S-phase cells visualized by EdU staining in the apical notches of 3-day-old gemmalings. The number of EdU signals in the apical notches of Mp*an-1*^{ko} was identical to that of Tak-1 (Fig. S9). Thus, cell proliferation is not altered in the Mp*an* knockout lines. In contrast, the apical notches of Mp*an-1*^{ko} were more open than those of Tak-1 (Fig. S9), suggesting an altered growth orientation.

Cell expansion in Mp*an* mutants

Cell expansion is important in tissue morphogenesis. We cultured thalli under weak blue light to stimulate and evaluate cell elongation. Thalli of Tak-1 and Mp*an-1*^{ko} elongated in the vertical direction against the plate surface (Fig. 6A-D). Mp*an-1*^{ko} had a more wavy and jagged thallus margin than that of Tak-1. To compare thallus elongation between Tak-1 and Mp*an-1*^{ko}, we measured the thallus length of samples mounted on a glass slide (Fig. 6E). Elongation along the growth axis of Mp*an-1*^{ko} was suppressed compared with that of Tak-1. This tendency was also seen under standard white light (Fig. 4, Fig. S7). On the other hand, the thickness of thalli did not show any significant difference between Tak-1 and Mp*an-1*^{ko} (Fig. S10). In addition, in this growth condition, cell proliferation levels were the same (Fig. S9C). Next, we observed cell morphology by scanning electron microscopy (Fig. 7). In Tak-1, most epidermal cells elongated along the growth direction (Fig. 7A-D), but the elongation of epidermal cells in Mp*an-1*^{ko} was suppressed (Fig. 7E-H), particularly around the air pore, resulting in epidermal cells of heterogeneous morphology. Statistical analysis confirmed these differences in epidermal cell elongation between Tak-1 and Mp*an-1*^{ko} (Fig. 7I-K). Mp*an-1*^{ko} showed greater circularity and a smaller surface area in epidermal cells and a broader cell elongation angle. Moreover, thalli of Tak-1 had a smooth flat surface, whereas those of Mp*an-1*^{ko} had a rough uneven surface (Fig. 7B,F). Epidermal cell morphologies were also observed in longitudinal sections (Fig. S11). Epidermal cells of Mp*an-1*^{ko} had smaller, longer and slightly thicker cells with greater circularity. These results suggest that MpAN controls both directional and non-directional cell expansion.

Orientation of cortical MTs in Mp*an* mutants

In *A. thaliana an* mutants, it is thought that morphological phenotypes such as altered cell expansion direction and irregular

Development (2018) 145, dev161398. doi:10.1242/dev.161398

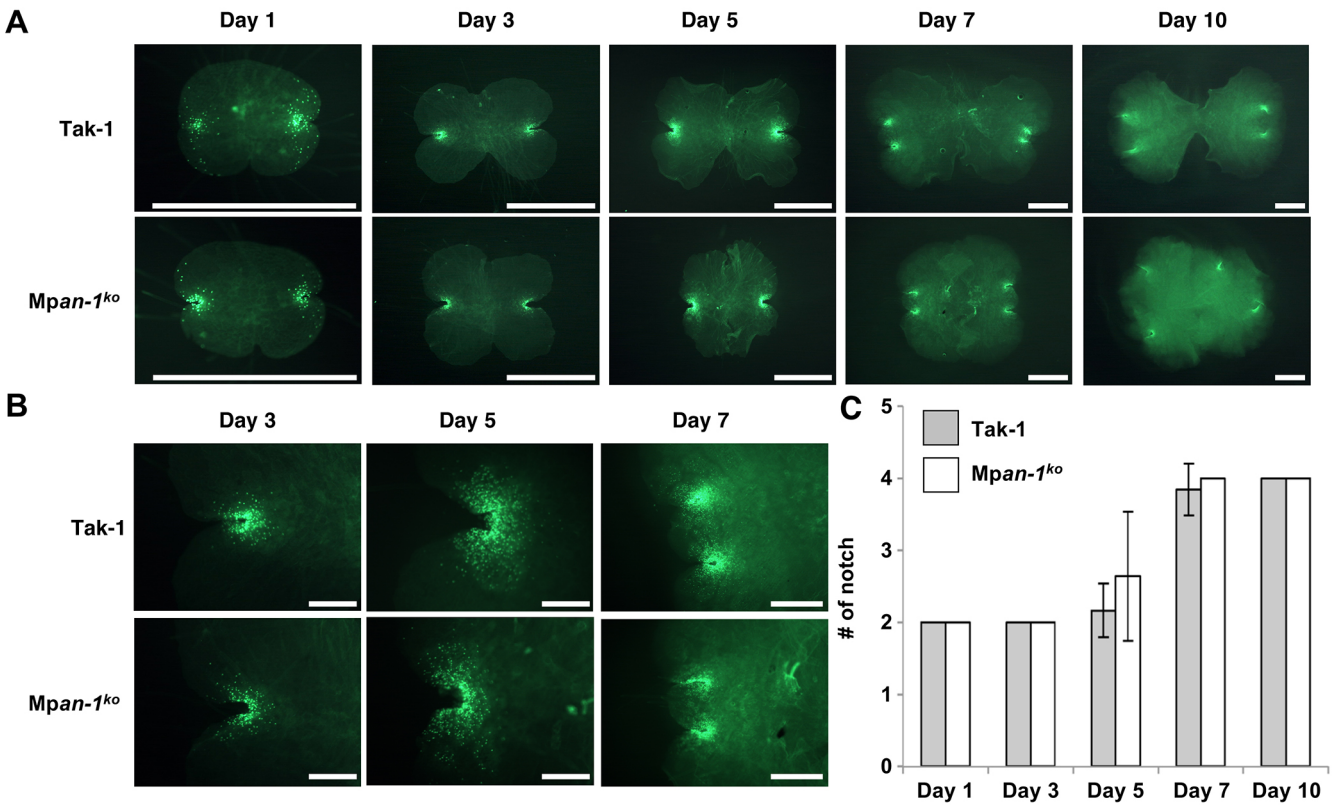

Fig. 5. Visualization of S-phase nuclei in Mp*an* mutants. (A,B) S-phase nuclei were visualized by EdU staining. Tak-1 and Mp*an-1*^{ko} (male) were treated with EdU-containing liquid medium for 2 h, mounted on slides with chloral hydrate and pressed lightly with a finger. A green signal indicates EdU incorporation into nuclei in whole plants (A) and around notches (B). Scale bars: 1 mm in A; 200 µm (3 and 5 days) and 500 µm (7 days) in B. (C) The number of notches in each thallus. Values are mean±s.d.; 13≤*n*≤18.

trichomes are caused by abnormal arrangement of cortical MTs (Kim et al., 2002; Folkers et al., 2002). Thus, we examined whether MpAN also affects the orientation of cortical MTs in the epidermal cells of elongated thalli by immunostaining using an anti-α-tubulin antibody (Fig. 8). Cortical MTs in Tak-1 were orientated mainly perpendicular to the growth direction and were aligned in parallel, whereas in Mp*an-1*^{ko}, they slightly tended to orientate along the growth direction. These MT orientations are coincident with epidermal cell morphology (Fig. 7). Thus, regulation of cortical MT arrangement by MpAN contributes to well-ordered thallus morphogenesis by controlling cell expansion in the gametophytes of liverworts. Moreover, we observed the subcellular localization of MpAN-Citrine driven by the Mp*AN* promoter (Fig. S12). MpAN-Citrine was observed as widely spread signal and diffuse punctate structures in the cytosol, similar to the GFP-fused AN localization in *A. thaliana* (Minamisawa et al., 2011; Bhasin and Hülskamp, 2017). The punctate structures of citrine signals were not colocalized with the TagRFP-TUB2 signal that visualizes MTs.

DISCUSSION

Roles of plant ANs in tissue morphogenesis

Although the molecular functions of AN were already known to be evolutionarily conserved among land plants in terms of whether homologs can complement the *an-1* mutation phenotypes of *A. thaliana* (Cho et al., 2005; Lin et al., 2008; Minamisawa et al., 2011), the roles of AN in the basal land plant *M. polymorpha* are unclear. Moreover, the roles of AN in the haploid gametophyte phase are unknown, because previous analyses have been restricted to diploid sporophytes of *A. thaliana*. In this study, to assess the roles of plant ANs in the haploid phase of basal land plants, we analyzed thallus development in Mp*an* knockout mutants of *M. polymorpha*. Mp*an* knockout mutants showed various morphological phenotypes, such as abnormal thalli that were twisted along the growth axis, suppressed thallus growth and an antheridial receptacle with a curled and wavy margin (Figs 1–4, Figs S4, S5, S7 and S8). This antheridial receptacle phenotype (Figs S4 and S5) and abnormal thalli may have similar causes, because the antheridial receptacle is similar in anatomy to the thallus (Shimamura, 2016). When the Mp*an* knockout lines were cultured under thallus-elongation conditions, suppressed elongation and an abnormal direction of epidermal cell expansion were apparent (Fig. 7, Fig. S11). Moreover, the knockout lines showed disordered cortical MT orientation (Fig. 8). Cortical MTs control the direction of cellulose microfibrils in the cell wall to determine the direction of cell expansion (Ledbetter and Porter, 1963; Paredez et al., 2006; Chen et al., 2016). These results suggest that MpAN coordinates the formation of well-ordered cell and tissue morphologies by regulating cortical MTs in gametophytes, similar to the situation in *A. thaliana* sporophytes.

Interestingly, the cortical MTs in leaf epidermal cells of *A. thaliana an* mutants were more regularly aligned in parallel compared with the wild-type lines (Kim et al., 2002; Folkers et al., 2002), whereas the thallus epidermal cells of the Mp*an* knockout mutants had more diverse orientations than those of the wild-type lines (Fig. 8). Although these phenomena appear to be opposing, *an* mutants in the two species share similar defects, i.e. the final cell morphogenesis are perturbed, because in the wild-type lines, the cell morphology differs markedly between leaf epidermis of *A. thaliana* and thallus epidermis of *M. polymorpha*. In fact, the organ-level

Development (2018) 145, dev161398. doi:10.1242/dev.161398

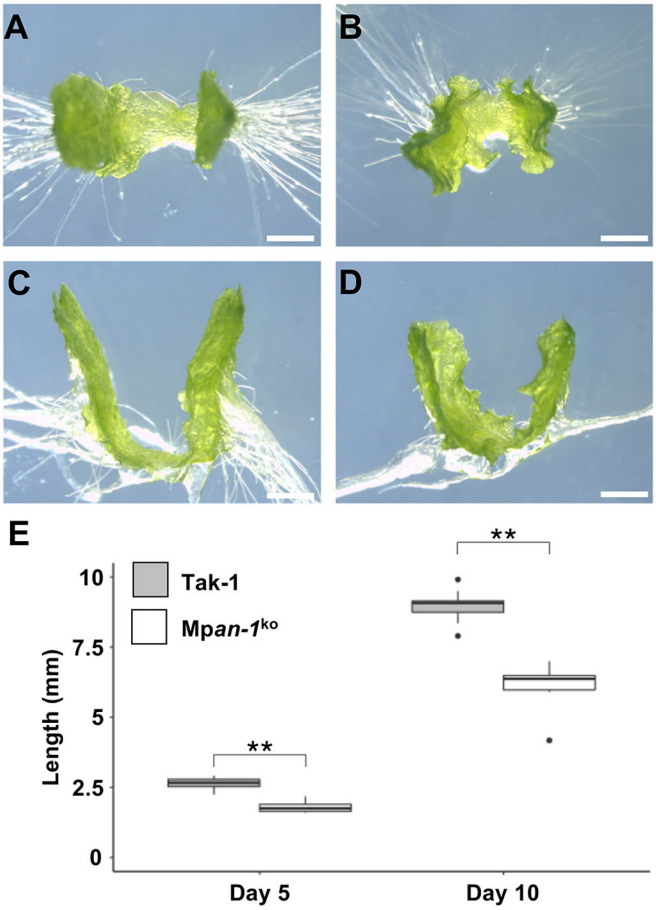

Fig. 6. Shapes of thalli in Mp*an* mutants under weak blue light. (A-D) Thallus shapes in Tak-1 (A,C) and Mp*an-1*^{ko} (male) (B,D) cultured for 10 days under weak blue light. Top (A,B) and side (C,D) views are shown. Scale bars: 1 mm. (E) The lengths of thalli cultured for 5 and 10 days are shown in box-and-whisker plots. Median values (middle bars) and first to third interquartile ranges (boxes); whiskers indicate 1.5× the interquartile ranges; dots indicate outliers; $n \geq 10$. $^{**}P<0.01$ compared with Tak-1; Student's *t*-test.

morphological phenotypes were similar between *A. thaliana* and *M. polymorpha*; i.e., Mp*an* knockout mutants formed twisted thalli (Figs 1-3), and the fruits, petals and roots of *A. thaliana an* mutants are twisted (Fulton et al., 2009; Bai et al., 2010, 2013; Kwak et al., 2015). *A. thaliana* with mutations in genes encoding tubulin and MT-associated proteins also show twisted (helical) growth in some organs (e.g. Smyth, 2016). In those mutants, the twisting orientations are fixed. Indeed, the twisting of thalli in Mp*an* knockout mutants was uniform and anti-clockwise. Therefore, MpAN and *A. thaliana* AN likely have similar functions in the regulation of cortical MT arrangement. How AN regulates the arrangement of cortical MTs is still unknown in *A. thaliana*. Further research on *M. polymorpha* will supply us with clues to discover its mechanism. A putative leucine-rich repeat receptor-like kinase, STRUBBELIG/SCRAMBLED (SUB/SCM), physically interacts with AN, and the *sub/scm* mutants share twisted phenotypes with *an* in *A. thaliana* (Fulton et al., 2009; Bai et al., 2013; Kwak et al., 2015). SUB belongs to the STRUBBELIG-RECEPTOR FAMILY (SRF) along with eight other members (SRF1-8) (Eyüboglu et al., 2007). We found one homolog, MpSUB (Mapoly0090s0074.1.p), in *M. polymorpha* using a blast search and phylogenic analysis. Further comparative research between MpAN and MpSUB will provide new clues to understanding the molecular function of plant ANs.

Recently, *A. thaliana* AN has been suggested to contribute to abiotic and biotic stress responses (Gachomo et al., 2013; Bhasin and Hülskamp, 2017). However, in this work we could not detect the clear differences in the response to various culture conditions (abiotic stresses and phytohormones) between the WT and the Mp*an* knockout mutant (Fig. S13).

Evolution of plant ANs

During land-plant evolution, regulatory genes were acquired to facilitate terrestrialization and development of 3D tissues, resulting in a more complex body plan (Graham et al., 2000; Ishizaki, 2017; Bowman et al., 2017). The molecular functions of AN in land plants are likely evolutionarily conserved, because all plant AN homologs can complement the *an-1* mutation phenotypes of *A. thaliana* (Cho et al., 2005; Lin et al., 2008; Minamisawa et al., 2011). In this study, we show that MpAN regulates the orientation of cortical MTs to ensure correct gametophyte morphogenesis. To our knowledge, this is the first report of the role of AN homologs in the haploid gametophyte phase. On the other hand, knockout of MpAN did not affect sporophyte morphogenesis (Fig. S6). Thus, these findings support the evolutionary conservation of the role of ANs as coordinators of tissue morphology at least in the dominant generations: the gametophyte phase in *M. polymorpha* and the sporophyte phase in *A. thaliana*, respectively. Genomic analysis of the filamentous charophyte *Klebsormidium nitens* suggests that an ancestor of *K. nitens* acquired genes related to organization of complex multicellular systems despite its simple body plan (Hori et al., 2014; Ohtaka et al., 2017). Indeed, the *K. nitens* genome harbors one AN homolog, but that of the single-celled Chlorophyta *Chlamydomonas reinhardtii* does not (Fig. S14). Although animal CtBPs and plant ANs evolved from NAD(H)-dependent D-hydroxyacid dehydrogenase (Stern et al., 2007), the molecular functions of animal CtBPs are distinct from those of plant ANs (Tsukaya, 2006; Stern et al., 2007). In brief, ancestral plant AN was derived from a D-hydroxyacid dehydrogenase in Charophyta; it co-opted to regulate cortical MT orientations (possibly in charophytes) and then contributed to 3D tissue morphology in the gametophytes of basal land plants. According to the evolution of land plants, specifically the transition in dominance from the gametophyte to sporophyte phases, the roles of AN in gametophyte morphogenesis in bryophytes may have been used for sporophyte morphogenesis in vascular plants.

MATERIALS AND METHODS

Plant materials and culture conditions

The *M. polymorpha* female accession Tak-2 and male accession Tak-1 were used as the wild-type lines (Ishizaki et al., 2008). Wild-type and transgenic plants were cultured on half-strength Gamborg's B5 medium (Gamborg et al., 1968) containing 1% (w/v) agar under 50-60 µmol m^{-2} s^{-1} continuous white light at 22°C. To induce the reproductive phase, 2-week-old thalli from gemmae cultured on half-strength Gamborg's B5 medium were transferred to rockwool and cultured under continuous 50-60 µmol m^{-2} s^{-1} white light supplemented with 20-40 µmol m^{-2} s^{-1} far-red light (730 nm) irradiation (VBL-T600-1, Valore). To induce elongation of thalli, wild-type and transgenic plants were cultured on half-strength Gamborg's B5 medium containing 1% (w/v) sucrose and 1% (w/v) agar under continuous 15 µmol m^{-2} s^{-1} blue light (470 nm) irradiation (LED-B, EYELA) at 22°C.

Vector construction

The MpAN targeting vector used for homologous recombination was constructed according to Ishizaki et al., (2013). The 5′ and 3′ ends of the 4.5 and 4.3 kb homologous arms of MpAN, respectively, were amplified from

Development (2018) 145, dev161398. doi:10.1242/dev.161398

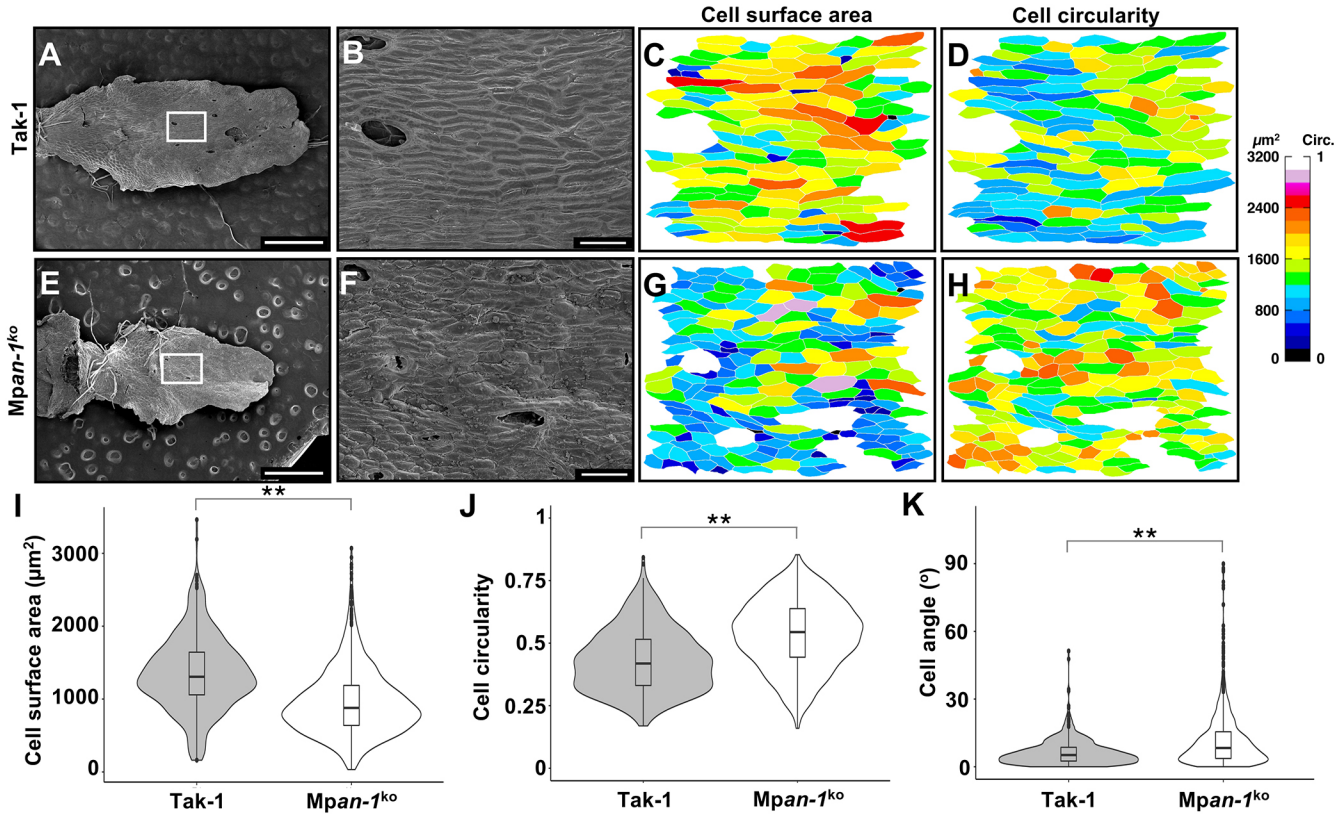

Fig. 7. Cell-surface area and circularity in Mp*an* mutants under weak blue light. (A,B,E,F) Scanning electron microscopy images of the surfaces of Tak-1 (A,B) and Mp*an-1*^{ko} (male) (E,F) cultured for 10 days under weak blue light. White boxes in A and E are magnified in B and F, respectively. Scale bars: 1 mm in A, E; and 100 µm in B,F. (C,D,G,H) Cell-surface area (C,G) and circularity (D,H) shown in scanning electron microscopy images (B,F) were measured. (I-K) Cell-surface area (I), circularity (J) and angle (K) values are shown in violin plots with box-and-whisker plots. Median values (middle bars) and first to third interquartile ranges (boxes); whiskers indicate 1.5× the interquartile ranges; dots indicate outliers; *n*=472 cells from three individuals (164, 167 and 141) for Tak-1, and *n*=981 cells from five individuals (261, 300, 161, 238 and 179) for Mp*an-1*^{ko}. ***P*<0.01 compared with Tak-1; Student's *t*-test.

Tak-1 genomic DNA by PCR using KOD FX Neo (Toyobo). To amplify the 5′ end, the forward primer 5′-CTA AGG TAG CGA TTA ATG TTT CAC AAA AGG CAA TAT TCA-3′ and reverse primer 5′-CCG GGC AAG CTT TTA ATG ACC GCC TTA TCA GCA CAA C-3′ were used. To amplify the 3′ end, the forward primer 5′-AAC ACT AGT GGC GCG CAC TCA AGC TCC GTC TAG GG-3′ and reverse primer 5′-TTA TCC CTA GGC GCG GAG GTG CGA TCT GGA AAA AC-3′ were used. The amplified 5′- and 3′-end fragments were cloned into the *Pac*I and *Asc*I sites of pJHY-TMp1 (Ishizaki et al., 2013), respectively, using the In-Fusion HD cloning kit (Clontech). MpAN-oligoA 5′-GCA CCC AGC CTC TCG CCT CCC GAG GCA TCG TCA GTT TTA GAG CTA GAA-3′ and MpAN-oligoB 5′-TTC TAG CTC TAA AAC TGA CGA TGC CTC GGG AGG CGA GAG GCT GGG TGC-3′ were incubated together at 95°C for 5 min to enable annealing. The annealed oligo was cloned into pMpGE_En01 digested with *Sac*I and *Pst*I using the In-Fusion HD cloning kit. The sequence between *attL1* and *attL2* within pMpGE_En01 was inserted into the binary vector pMpGE010 by LR reaction using LR clonase II (Life Technologies) (Sugano et al., 2018). The vector used for complementation analysis was constructed based on that of Ishizaki et al. (2015). The genomic sequence from the putative promoter region (5 kb upstream of the start codon) to the terminator region (1 kb downstream of the stop codon) of MpAN was amplified from Tak-1 genomic DNA by PCR using KOD FX Neo (Toyobo) with the following primer pairs: proMpAN-Fw 5′-CAC CAG AGT TTG TAT GTA CAG CGG-3′ and tarMpAN-Rev 5′-ACA GGA TCC TAG TTG AGG AC-3′. The PCR product, *proMpAN:MpAN:tarMpAN*, was cloned into pENTR/D-TOPO (Life Technologies). The plant-specific C-terminal region deleted entry vector was constructed by mutagenesis on pENTR/D-TOPO-*pro*Mp*AN:*Mp*AN:tarMpAN* using the following primer pair: 5′-AAA AGC CTA GTT TAC GTT ATG GAT GAT-3′ and 5′-GTA AAC TAG GCT TTT CGT CGC CCT GCT CTT-3′. The region between *attL1* and *attL2* within the entry vectors were inserted into the destination vector pMpGWB301 (Ishizaki et al., 2015) by LR reaction using LR clonase II (Life Technologies). The promoter:reporter fusion constructs *pro*Mp*AN:GUS* and *pro*Mp*AN:Citrine-NLS* were also constructed based on those of Ishizaki et al. (2015). The 5 kb promoter region of MpAN was amplified using proMpAN-Fw as described above and proMpAN-Rev 5′-TGC CAG TTC AGT AAT GCC TAC C-3′, and cloned into pENTR/D-TOPO. The constructed entry vector was used for LR cloning with the destination vectors pMpGWB304 and pMpGWB315 (Ishizaki et al., 2015). pENTR/D-TOPO-*pro*Mp*AN:*Mp*AN* was constructed by mutagenesis on pENTR/D-TOPO-*pro*Mp*AN:*Mp*AN:tarMpAN* using the following primer pair: 5′-GCT TAG CAA GGG TGG GCG CGC CGA C-3′ and 5′-CCA CCC TTG CTA AGC CAG CGT ACT A-3′. The constructed entry vector was used for LR cloning with the destination vector pMpGWB307 for the *pro*Mp*AN:MpAN-Citrine* construct (Ishizaki et al., 2015).

Agrobacterium-mediated transformation

The transformation procedures for homologous recombination, the CRISPR/Cas9 system, and the promoter:reporter fusion constructs were performed as described previously (Ishizaki et al., 2008) using spores obtained by crossing Tak-2 with Tak-1. Transformants were selected on half-strength B5 agar medium containing 1% (w/v) agar, 10 mg l^{-1} hygromycin (Wako Pure Chemical Industries) and 100 mg l^{-1} cefotaxime (Claforan; Sanofi-Aventis). Two Mp*an* knockout lines, a female (#49) and a male (#121), constructed by homologous recombination were isolated. These Mp*an* knockout lines were crossed to generate F1 spores. After spore germination, a female and male line were again isolated. In this study, Mp*an-1*^{ko} (female) and Mp*an-1*^{ko} (male) were used. Thallus transformation was performed as described previously (Kubota et al., 2013). Thalli from

Development (2018) 145, dev161398. doi:10.1242/dev.161398

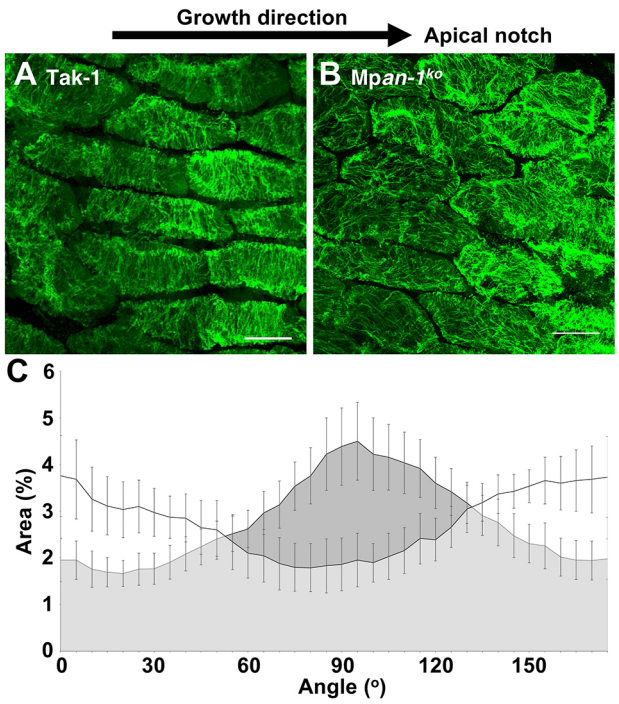

Fig. 8. Arrangement of cortical MTs in Mp*an* mutants under weak blue light. (A,B) Cortical MTs in epidermal cells from Tak-1 (A) and Mp*an-1*^{ko} (male) (B) cultured for 10 days under weak blue light were visualized by immunostaining using an anti-α-tubulin antibody. Scale bars: 20 µm. (C) Orientation of cortical MTs was analyzed using a mathematical morphology method. Values are mean±s.d.; *n*=6 images from three individuals each.

Mp*an-1*^{ko} (female) and/or Mp*an-1*^{ko} (male), and *Agrobacterium* containing the pMpGWB301-*pro*Mp*AN:*Mp*AN:tar*Mp*AN* vector, the pMpGWB301-*pro*Mp*AN:*Mp*AN ΔCT:tar*Mp*AN* vector or the pMpGWB307-*pro*Mp*AN:*Mp*AN* vector were used for transformation. pMpGWB304-*pro*Mp*AN* and pMpGWB315-*pro*Mp*AN* were transformed to Tak-1 and Tak-2. Additionally, the pMpGWB307-*pro*Mp*AN:*Mp*AN* vector and the pMpGWB202-*TagRFP-MpTUB2* vector for the *CaMV35Spro:TagRFP-MpTUB2* construct (Otani et al., 2018) were co-transfomed to Mp*an-1*^{ko} (male). Transformants were selected on half-strength B5 agar medium containing 1% (w/v) agar, 0.5 µM chlorsulfuron and 100 mg l^{-1} cefotaxime (Claforan; Sanofi-Aventis).

Genomic PCR

Genomic DNA extraction from thalli and genomic PCR were performed as described previously (Ishizaki et al., 2013). To verify the Mp*an* knockout and Mp*an* genome-edited lines, the following primer pairs were used: MpAN-a 5′-GGT AGG CAT TAC TGA ACT GGC A-3′ and MpAN-b 5′-TTT TCA CCA AAG GTG GGA AG-3′. The primer sets for the sex chromosome-specific DNA markers rbm27, rhf73 and rbf62 were as described previously (Fujisawa et al., 2001).

RT-PCR

Total RNAs were extracted using an RNeasy Plant Mini Kit (Qiagen). cDNAs were synthesized from the extracted RNAs using a PrimeScript RT reagent kit (TAKARA). Mp*AN* transcripts were amplified using the forward primer 5′-AAG GGT TCT GGA AAA AAG GG-3′ and the reverse primer 5′-GCT AAG CCA GCG TAC TCC A-3′. Mp*EF1α* transcripts were amplified using the forward primer 5′-TCA CTC TGG GTG TGA AGC AG -3′ and the reverse primer 5′-GCC TCG ACT AAA GCT TCG TG-3′. The PCR was performed using Quick *Taq* HS DyeMix (TOYOBO).

GUS staining

GUS staining of thalli *pro*Mp*AN:GUS* transgenic plants was performed as described previously (Althoff et al., 2014).

EdU staining

To visualize S-phase cells, the Click-iT EdU Imaging Kit (Life Technologies) was used. Gemmalings cultured for several days were soaked in half-strength Gamborg's B5 medium with 10 µM EdU at 22°C for 2 h under continuous white light. Thalli were fixed in FAA [50% (v/v) ethyl alcohol, 2.5% (w/v) glacial acetic acid, and 2.5% (w/v) formalin] and were degassed by centrifugation at 10,000 ***g*** for 10 s. The fixed samples were stained for EdU with Alexa Fluor 488-azide as described previously (Yin and Tsukaya, 2016). Samples were mounted on glass slides with chloral hydrate solution (200 g chloral hydrate, 20 g glycerol and 50 ml dH_2O). Alexa Fluor 488 fluorescence was visualized using the M16F fluorescence microscope (Leica) at excitation and detection wavelengths of 488 and 519 nm, respectively.

EdU and mPS-PI staining

Three-day-old gemmalings were soaked in half-strength Gamborg's B5 medium with 10 µM EdU at 22°C for 1 h under continuous white light. The samples were fixed in 50% (v/v) methyl alcohol and 10% (v/v) acetic acid and were degassed at 10,000 ***g*** for 10 s. Samples in fixative solution were incubated at 4°C for at least 12 h. After fixation, the samples were incubated in 80%, 90% and 100% (v/v) ethanol and 90% (v/v) acetone at 80°C for 5 min each, followed by fixative solution at 22°C for 30 min. After four washes with 0.5% (v/v) Triton X-100 in PBS, samples were incubated with an EdU detection cocktail for 30 min in the dark. The samples were rinsed with 0.5% (v/v) Triton X-100 in PBS and incubated in 1% (w/v) periodic acid at 22°C for 45 min. The samples were rinsed again with 0.5% (v/v) Triton X-100 in PBS and incubated in 0.1 mg ml^{-1} propidium iodide solution for 1 h. After four washes with 0.5% (v/v) Triton X-100 in PBS, the samples were transferred onto slides and incubated with chloral hydrate solution for 30 min. Before observation, a coverslip was placed on top of the samples. Alexa Fluor 488 fluorescence and propidium iodide were visualized using the FV1000 confocal laser scanning microscope (Olympus). *Z*-series fluorescence images in 2 µm steps were obtained at excitation and detection wavelengths of 473 and 490-540 nm for Alexa Fluor 488, and at 559 and 575-675 nm for propidium iodide, respectively. *Z*-projection images were created using ImageJ software (Schneider et al., 2012).

Micro-CT imaging

Micro-CT images of 10-day-old gemmalings cultured on half-strength Gamborg's B5 medium were obtained using the R_mCT2 micro-CT system (Rigaku) at 90 kV (180 µA) for 4.5 min with a 13 mm field of view. 3D images were reconstructed using OsiriX software (Pixmeo).

Scanning electron microscopy

Samples fixed in FAA were dehydrated through a graded ethanol series and isoamyl acetate, and dried using the JCPD-5 critical point dryer (JEOL). The samples were mounted using carbon tape and coated with platinum using the JEC-3000FC sputter-coater (JEOL). Images of epidermal cell surfaces were captured using the JSM-6510LV scanning electron microscope (JEOL). Epidermal cell margins were traced using Photoshop software (Adobe) and analyzed using ImageJ software.

Sectioning

Gemmalings were fixed overnight in FAA [50% (v/v) ethyl alcohol, 2.5% (w/v) glacial acetic acid and 2.5% (w/v) formalin] and were degassed. The fixed samples were incubated in 70%, 90% and 100% (v/v) ethanol for 10 min each, followed by 100% (v/v) ethanol for 20 min. Dehydrated samples were then preincubated in a solution of 50% (v/v) Technovit 7100 (Kulzer) for 30 min and in 100% Technovit resin for 30 min. The samples were incubated in 100% resin with 0.05% (w/v) Neutral Red overnight. The samples were embedded in Technovit resin following the manufacturer's protocol. Sections of 7 µm were cut with the HM360 microtome (MICROM), stained with Toluidine Blue and photographed using a DM4500 light microscope (Leica).

Immunostaining

Microtubules were visualized based on methods used in previous publication (Pasternak et al., 2015). Gemmalings were transferred into 2% (w/v) paraformaldehyde in PEMT buffer [50 mM PIPES, 2 mM EGTA,

2 mM $MgSO_4$, and 0.05% (v/v) Triton X-100 (pH 7.2)]. After degassing, the samples were incubated for 40 min at 37°C with gentle shaking. After three washes with water, the water was replaced with 100% methanol and the samples were incubated at 60°C for 10 min. Water was gradually added until a methanol concentration of 20% was reached, and the samples were rinsed again with water. The samples were then incubated in cell-wall digestion solution [0.2% (w/v) driselase and 0.15% (w/v) macerozyme in 2 mM MES (pH 5.0)] at 37°C for 40 min. After three washes with PBS with 0.1% (v/v) Triton X-100 (PBSTX), the samples were treated with membrane-permeabilization solution [3% (v/v) IGEPAL C630, 10% (v/v) dimethylsulfoxide in PBS] at 37°C for 20 min and rinsed four times with PBSTX. The samples were blocked in blocking buffer [2% (w/v) bovine serum albumin in PBSTX] for 30 min and incubated at 37°C for 1 h in blocking buffer containing 1000-fold diluted anti-α-tubulin antibody (Sigma T5168). After three washes with PBSTX, the samples were incubated at 37°C for 1 h with 500-fold-diluted anti-mouse IgG (H+L) secondary antibody conjugated to Alexa Fluor 488 (Thermo Fisher A-11017). *Z*-series images of Alexa Fluor 488 fluorescence were captured in 0.1 µm steps using the FV1000 confocal laser scanning microscope (Olympus). Cortical MT orientation was quantified using a mathematical morphology method described previously (Kimori et al., 2016).

Acknowledgements
We thank Dr Akihiro Fujikawa for assistance with the micro-CT scanning (National Institute for Basic Biology); Dr Yuki Kondo (The University of Tokyo) for assistance with the confocal microscopy, and his helpful and kind support; Dr Hiroyuki Koga (The University of Tokyo) for assistance with the immunostaining; and Emma Sarath (The University of Tokyo) for support with manuscript preparation.

Competing interests
The authors declare no competing or financial interests.

Author contributions
Methodology: T.F., Y.K., R.N., T.K.; Investigation: T.F., K.H.; Resources: S.I., R.N., T.K.; Writing - original draft: T.F., R.N., T.K., H.T.; Writing - review & editing: T.F., K.H., Y.K., S.I., R.N., T.K., H.T.; Supervision: H.T.; Funding acquisition: T.K., H.T.

Funding
This work was supported by the Ministry of Education, Culture, Sports, Science, and Technology, Japan (Scientific Research on Priority Areas and Scientific Research on Innovative Areas) (25113001 to H.T. and 25113009 to T.K.). Part of this study was supported by a National Institute for Basic Biology Priority Collaborative Research Project (17-526).

Supplementary information
Supplementary information available online at
http://dev.biologists.org/lookup/doi/10.1242/dev.161398.supplemental

References
Althoff, F., Kopischke, S., Zobell, O., Ide, K., Ishizaki, K., Kohchi, T. and Zachgo, S. (2014). Comparison of the *MpEF1α* and *CaMV35* promoters for application in *Marchantia polymorpha* overexpression studies. *Transgenic Res.* **23**, 235-244.

Bai, Y., Falk, S., Schnittger, A., Jakoby, M. J. and Hülskamp, M. (2010). Tissue layer specific regulation of leaf length and width in Arabidopsis as revealed by the cell autonomous action of *ANGUSTIFOLIA*. *Plant J.* **61**, 191-199.

Bai, Y., Vaddepalli, P., Fulton, L., Bhasin, H., Hülskamp, M. and Schneitz, K. (2013). *ANGUSTIFOLIA* is a central component of tissue morphogenesis mediated by the atypical receptor-like kinase STRUBBELIG. *BMC Plant Biol.* **13**, 16.

Bhasin, H. and Hülskamp, M. (2017). ANGUSTIFOLIA, a plant homolog of CtBP/BARS localizes to stress granules and regulates their formation. *Front. Plant Sci.* **8**, 1004.

Bowman, J. L., Kohchi, T., Yamato, K. T., Jenkins, J., Shu, S., Ishizaki, K., Yamaoka, S., Nishihama, R., Nakamura, Y., Berger, F. et al. (2017). Insights into land plant evolution garnered from the *Marchantia polymorpha* genome. *Cell* **171**, 287-304.

Chen, X., Wu, S., Liu, Z. and Friml, J. (2016). Environmental and endogenous control of cortical microtubule orientation. *Trends Cell Biol.* **26**, 409-419.

Chinnadurai, G. (2007). Transcriptional regulation by C-terminal binding proteins. *Int. J. Biochem. Cell Biol.* **39**, 1593-1607.

Cho, K.-H., Shindo, T., Kim, G.-T., Nitasaka, E. and Tsukaya, H. (2005). Characterization of a member of the AN subfamily, IAN, from *Ipomoea nil*. *Plant Cell Physiol.* **46**, 250-255.

Cho, K.-H., Tsukaya, H. and Kim, G.-T. (2008). Characterization of a dehydrogenase motif and an uORF in *Arabidopsis ANGUSTIFOLIA* gene. *Plant Biotech.* **25**, 365-368.

Eyüboglu, B., Pfister, K., Haberer, G., Chevalier, D., Fuchs, A., Mayer, K. F. X. and Schneitz, K. (2007). Molecular characterisation of the *STRUBBELIG-RECEPTOR FAMILY* of genes encoding putative leucine-rich repeat receptor-like kinases in *Arabidopsis thaliana*. *BMC Plant Biol.* **7**, 16.

Folkers, U., Kirik, V., Schöbinger, U., Falk, S., Krishnakumar, S., Pollock, M. A., Oppenheimer, D. G., Day, I., Reddy, A. S., Jürgens, G. et al. (2002). The cell morphogenesis gene *ANGUSTIFOLIA* encodes a CtBP/BARS-like protein and is involved in the control of the microtubule cytoskeleton. *EMBO J.* **21**, 1280-1288.

Fujisawa, M., Hayashi, K., Nishio, T., Bando, T., Okada, S., Yamato, K. T., Fukuzawa, H. and Ohyama, K. (2001). Isolation of X and Y chromosome-specific DNA markers from a liverwort, *Marchantia polymorpha*, by representational difference analysis. *Genetics* **159**, 981-985.

Fulton, L., Batoux, M., Vaddepalli, P., Yadav, R. K., Busch, W., Andersen, S. U., Jeong, S., Lohmann, J. U. and Schneitz, K. (2009). *DETORQUEO*, *QUIRKY*, and *ZERZAUST* represent novel components involved in organ development mediated by the receptor-like kinase STRUBBELIG in *Arabidopsis thaliana*. *PLoS Genet.* **5**, e1000355.

Gachomo, E. W., Jimenez-Lopez, J. C., Smith, S. R., Cooksey, A. B., Oghoghomeh, O. M., Johnson, N., Baba-Moussa, L. and Kotchoni, S. O. (2013). The cell morphogenesis *ANGUSTIFOLIA* (*AN*) gene, a plant homolog of CtBP/BARS, is involved in abiotic and biotic stress response in higher plants. *BMC Plant Biol.* **13**, 79.

Gamborg, O. L., Miller, R. A. and Ojima, K. (1968). Nutrient requirements of suspension cultures of soybean root cells. *Exp. Cell Res.* **50**, 151-158.

Graham, L. E., Cook, M. E. and Busse, J. S. (2000). The origin of plants: body plan changes contributing to a major evolutionary radiation. *Proc. Natl. Acad. Sci. USA* **97**, 4535-4540.

Hori, K., Maruyama, F., Fujisawa, T., Togashi, T., Yamamoto, N., Seo, M., Sato, S., Yamada, T., Mori, H., Tajima, N. et al. (2014). *Klebsormidium flaccidum* genome reveals primary factors for plant terrestrial adaptation. *Nat. Commun.* 5, 3978.

Hülskamp, M., Misŕa, S. and Jürgens, G. (1994). Genetic dissection of trichome cell development in *Arabidopsis*. *Cell* **76**, 555-566.

Ishizaki, K. (2017). Evolution of land plants: insights from molecular studies on basal lineages. *Biosci. Biotechnol. Biochem.* **81**, 73-80.

Ishizaki, K., Chiyoda, S., Yamato, K. T. and Kohchi, T. (2008). *Agrobacterium*-mediated transformation of the haploid liverwort *Marchantia polymorpha* L., an emerging model for plant biology. *Plant Cell Physiol.* **49**, 1084-1091.

Ishizaki, K., Johzuka-Hisatomi, Y., Ishida, S., Iida, S. and Kohchi, T. (2013). Homologous recombination-mediated gene targeting in the liverwort *Marchantia polymorpha* L. *Sci. Rep.* **3**, 1532.

Ishizaki, K., Nishihama, R., Ueda, M., Inoue, K., Ishida, S., Nishimura, Y., Shikanai, T. and Kohchi, T. (2015). Development of gateway binary vector series with four different selection markers for the liverwort *Marchantia polymorpha*. *PLoS ONE* **10**, e0138876.

Ishizaki, K., Nishihama, R., Yamato, K. T. and Kohchi, T. (2016). Molecular genetic tools and techniques for *Marchantia polymorpha* research. *Plant Cell Physiol.* **57**, 262-270.

Kim, G.-T., Shoda, K., Tsuge, T., Cho, K.-H., Uchimiya, H., Yokoyama, R., Nishitani, K. and Tsukaya, H. (2002). The *ANGUSTIFOLIA* gene of *Arabidopsis*, a plant *CtBP* gene, regulates leaf-cell expansion, the arrangement of cortical microtubules in leaf cells and expression of a gene involved in cell-wall formation. *EMBO J.* **21**, 1267-1279.

Kimori, Y., Hikino, K., Nishimura, M. and Mano, S. (2016). Quantifying morphological features of actin cytoskeletal filaments in plant cells based on mathematical morphology. *J. Theor. Biol.* **389**, 123-131.

Kubota, A., Ishizaki, K., Hosaka, M. and Kohchi, T. (2013). Efficient *agrobacterium*-mediated transformation of the liverwort *Marchantia polymorpha* using regenerating thalli. *Biosci. Biotechnol. Biochem.* **77**, 167-172.

Kwak, S.-H., Song, S.-K., Lee, M. M. and Schiefelbein, J. (2015). ANGUSTIFOLIA mediates one of the multiple SCRAMBLED signaling pathways regulating cell growth pattern in *Arabidopsis thaliana*. *Biochem. Biophys. Res. Commun.* **465**, 587-593.

Ledbetter, M. C. and Porter, K. R. (1963). A microtubule in plant cell fine structure. *J. Cell Biol.* **19**, 239-250.

Lin, X., Minamisawa, N., Takechi, K., Zhang, W., Sato, H., Takio, S., Tsukaya, H. and Takano, H. (2008). Isolation and characterization of the *Larix gmelinii ANGUSTIFOLIA* (*LgAN*) gene. *Planta* **228**, 601-608.

Minamisawa, N., Sato, M., Cho, K.-H., Ueno, H., Takechi, K., Kajikawa, M., Yamato, K. T., Ohyama, K., Toyooka, K., Kim, G.-T. et al. (2011). ANGUSTIFOLIA, a plant homolog of CtBP/BARS, functions outside the nucleus. *Plant J.* **68**, 788-799.

Nishihama, R., Ishizaki, K., Hosaka, M., Matsuda, Y., Kubota, A. and Kohchi, T. (2015). Phytochrome-mediated regulation of cell division and growth during regeneration and sporeling development in the liverwort *Marchantia polymorpha*. *J. Plant Res.* **128**, 407-421.

Ohtaka, K., Hori, K., Kanno, Y., Seo, M. and Ohta, H. (2017). Primitive auxin response without TIR1 and Aux/IAA in the Charophyte Alga *Klebsormidium nitens*. *Plant Physiol.* **174**, 1621-1632.

Otani, K., Ishizaki, K., Nishihama, R., Takatani, S., Kohchi, T., Takahashi, T. and Motose, H. (2018). An evolutionarily conserved NIMA-related kinase directs rhizoid tip growth in the basal land plant *Marchantia polymorpha*. *Development* **145**, dev154617.

Paredez, A. R., Somerville, C. R. and Ehrhardt, D. W. (2006). Visualization of cellulose synthase demonstrates functional association with microtubules. *Science* **312**, 1491-1495.

Pasternak, T., Tietz, O., Rapp, K., Begheldo, M., Nitschke, R., Ruperti, B. and Palme, K. (2015). Protocol: an improved and universal procedure for whole-mount immunolocalization in plants. *Plant Methods* **11**, 50.

Rédei, G. P. (1962). Single locus heterosis. *Zeitschrift für Vererbungslehre* **93**, 164-170.

Schneider, C. A., Rasband, W. S. and Eliceiri, K. W. (2012). NIH Image to ImageJ: 25 years of image analysis. *Nat. Methods* **9**, 671-675.

Shimamura, M. (2016). *Marchantia polymorpha*: taxonomy, phylogeny and morphology of a model system. *Plant Cell Physiol.* **57**, 230-256.

Smyth, D. R. (2016). Helical growth in plant organs: mechanisms and significance. *Development* **143**, 3272-3282.

Solly, J. E., Cunniffe, N. J. and Harrison, C. J. (2017). Regional growth rate differences specified by apical notch activities regulate liverwort thallus shape. *Curr. Biol.* **27**, 16-26.

Stern, M. D., Aihara, H., Cho, K.-H., Kim, G.-T., Horiguchi, G., Roccaro, G. A., Guevara, E., Sun, H. H., Negeri, D., Tsukaya, H. et al. (2007). Structurally related *Arabidopsis* ANGUSTIFOLIA is functionally distinct from the transcriptional corepressor CtBP. *Dev. Genes Evol.* **217**, 759-769.

Sugano, S. S., Nishihama, R., Shirakawa, M., Takagi, J., Matsuda, Y., Ishida, S., Shimada, T., Hara-Nishimura, I., Osakabe, K. and Kohchi, T. (2018). Efficient CRISPR/Cas9-based genome editing and its application to conditional genetic analysis in *Marchantia polymorpha*. *bioRxiv*. doi:https://doi.org/10.1101/277350.

Tsuge, T., Tsukaya, H. and Uchimiya, H. (1996). Two independent and polarized processes of cell elongation regulate leaf blade expansion in *Arabidopsis thaliana* (L.) Heynh. *Development* **122**, 1589-1600.

Tsukaya, H. (2006). A new member of the CtBP/BARS family from plants: angustifolia. In *CtBP Family Protein* (ed. G. Chinnadurai), pp. 112-118. Georgetown, Texas: Landes Bioscience.

Tsukaya, H., Tsuge, T. and Uchimiya, H. (1994). The cotyledon: a superior system for studies of leaf development. *Planta* **195**, 309-312.

Wickett, N. J., Mirarab, S., Nguyen, N., Warnow, T., Carpenter, E., Matasci, N., Ayyampalayam, S., Barker, M. S., Burleigh, J. G., Gitzendanner, M. A. et al. (2014). Phylotranscriptomic analysis of the origin and early diversification of land plants. *Proc. Natl. Acad. Sci. USA* **111**, 4859-4868.

Yin, X. and Tsukaya, H. (2016). A pulse-chase strategy for EdU labelling assay is able to rapidly quantify cell division orientation. *New Phytol.* **211**, 1462-1469.

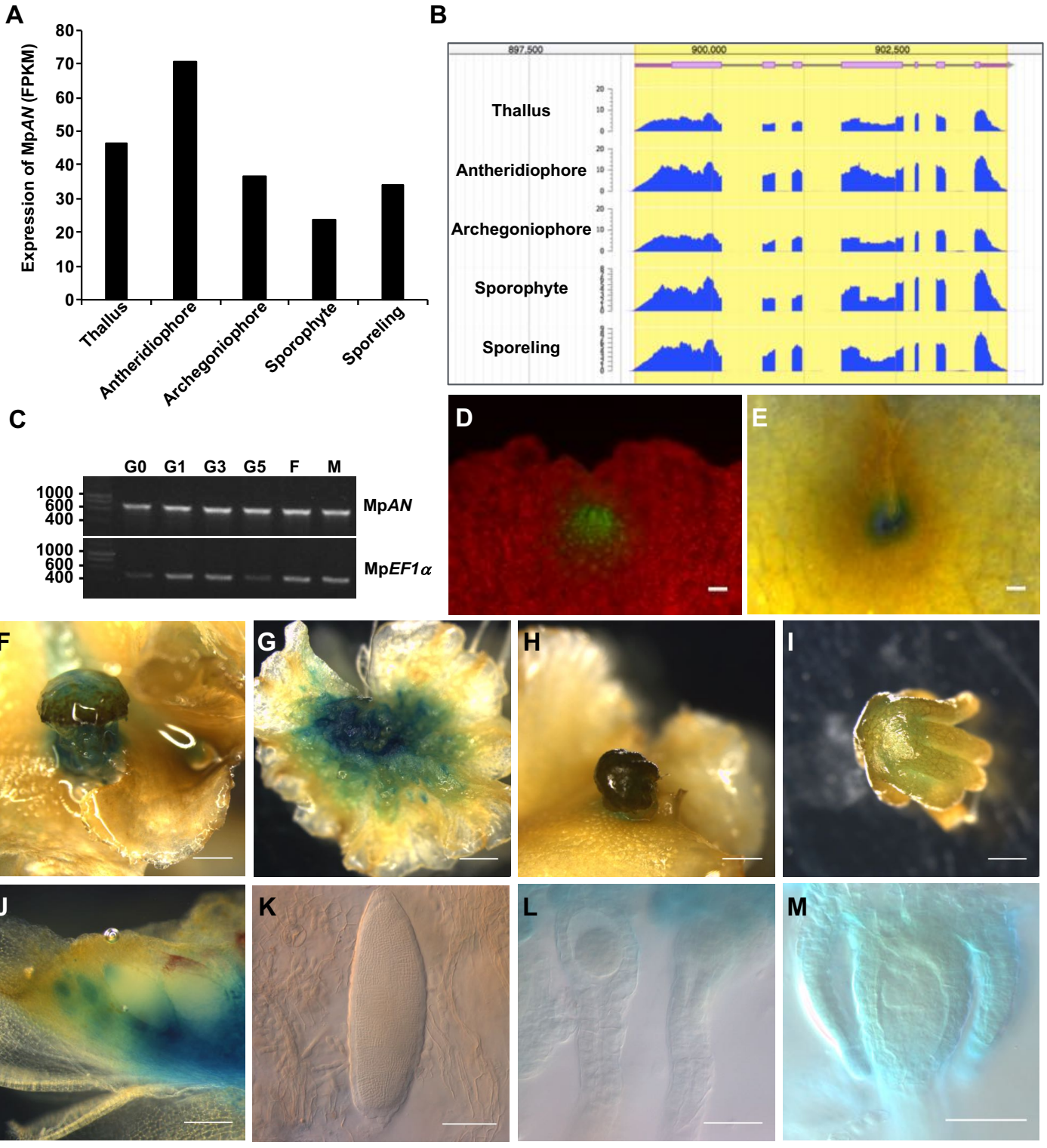

Fig. S1. Expression pattern of Mp*AN* gene. (A, B) Expression levels (A) and expression profiles (B) of Mp*AN* gene in various organs were extracted and visualized from the published RNA-seq data sets in Bowman et al., 2017 and the genome database for *M.polymorpha*, MarpolBase. (C) Expression levels of Mp*AN* gene during gemmae, gemmalings, and developing antheridiophores and archegoniophores were analyzed by using RT-PCR. Expression levels of Mp*EF1α* were also indicated as a control. Total RNAs were extracted from gemmae indicated as G0, genmalings cultured for 1, 3, and 5 days indicated as G1, G3, and G5, and developing archegoniophores and antheridiophores indicated as F and M, respectively. (D, E) Expression pattern of *p*Mp*AN:Citrine-NLS* (D) and *p*Mp*AN:GUS-10* (E) in thallus of T1 transgenic plants were visualized. Citrine signals are shown in green and autofluorescence in red (D). (F, G, H, I, J, K, L) Expression pattern of *p*Mp*AN:GUS-10* (male) (F, G, J, K) and *p*Mp*AN:GUS-4* (female) (H, I, L) in reproductive organs were visualized. The early developmental stage of antheridiophores (F) and archegoniophores (H). Antheridial receptacle (G) and archegonial receptacle (I). Free-hand vertical section views of antheridial receptacle (J). Antheridium (K) and archegonium (L). Embryo of *p*Mp*AN:GUS-4* (female) with *p*Mp*AN:GUS-10* (male) (M). Bars, 100 μm (E, D), 1 mm (F-I), 200 μm (J), 100 μm (K), 50 μm (L, M).

A

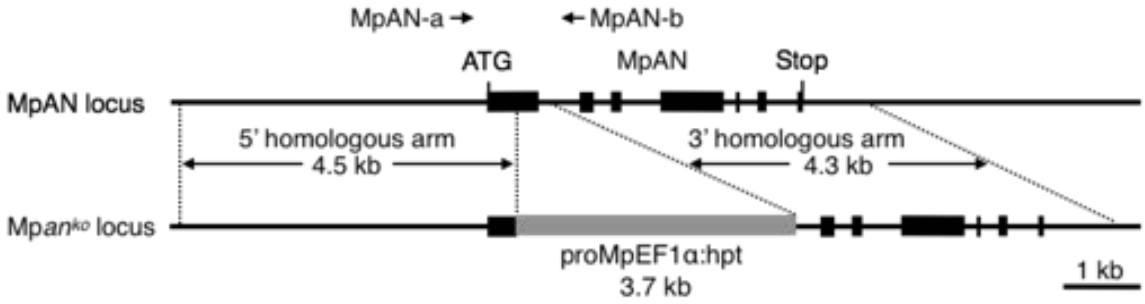

B

```
AA          M  G  K  G  V  T  M  P  P  E  A  S                    S  G  R
Tak-1       ATGGGCAAGGGCGTCACGATGCCTCCCGAGGCATCG----------------TCAGGGA  43
Mpan-4ge    ATGGGCAAGGGCGTCACGATGCCTCCCGAGGCATCGTAAACCCCCATCCACCCTCAGGGA  60
Mpan-9ge    ATGGGCAAGGGCGTCACGATGCCTCCCGA----------------------------  29

AA            V  D  G  G  R  V  A  E  R  N  P  G  S  R  Q  I  G  K  M  R
Tak-1       GGGTGGATGGGGGTAGGGTAGCGGAGAGAAATCCTGGTTCGCGGCAAATTGGAAAGATGC 103
Mpan-4ge    GGGTGGATGGGGGTAGGGTAGCGGAGAGAAATCCTGGTTCGCGGCAAATTGGAAAGATGC 120
Mpan-9ge    ------------------------------------------------------------  29

AA            S  D  G  T  V  R  K  S  K  G  Y  E  P  L  S  M  G  L  P  L
Tak-1       GGAGCGACGGGACTGTGAGGAAGTCAAAAGGTTACGAACCGCTCAGCATGGGATTACCTC 163
Mpan-4ge    GGAGCGACGGGACTGTGAGGAAGTCAAAAGGTTACGAACCGCTCAGCATGGGATTACCTC 180
Mpan-9ge    ------------------------------------------------------------  29

AA            V  V  A  L  N  C  M  D  D  C  R  A  E  A  E  A  L  E  G  V
Tak-1       TGGTCGTGGCTCTGAATTGCATGGACGATTGTCGTGCCGAAGCCGAGGCTTTGGAAGGAG 223
Mpan-4ge    TGGTCGTGGCTCTGAATTGCATGGACGATTGTCGTGCCGAAGCCGAGGCTTTGGAAGGAG 240
Mpan-9ge    ------------------------------------------------------------  29

AA            A  V  V  E  H  V  G  L  A  Q  V  G  E  G  K  I  E  A  A  V
Tak-1       TGGCTGTAGTTGAGCATGTGGGTCTCGCCCAGGTTGGAGAAGGAAAGATCGAAGCGGCCG 283
Mpan-4ge    TGGCTGTAGTTGAGCATGTGGGTCTCGCCCAGGTTGGAGAAGGAAAGATCGAAGCGGCCG 300
Mpan-9ge    --------------------GGTCTCGCCCAGGTTGGAGAAGGAAAGATCGAAGCGGCCG  69
```

C

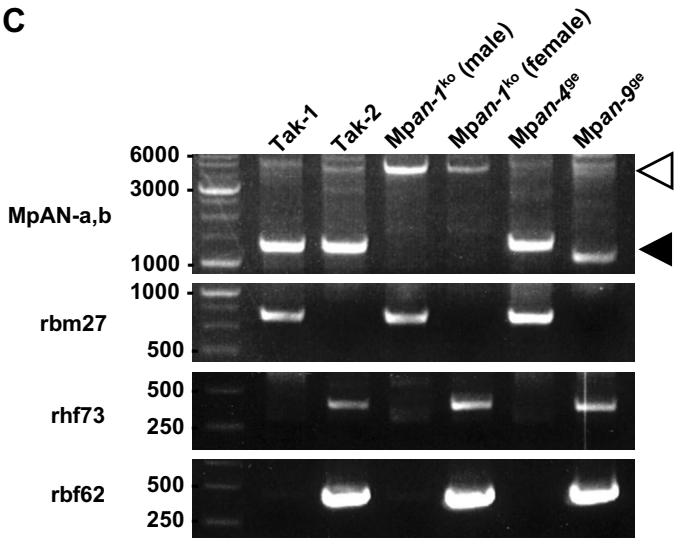

Fig. S2. Construction of Mp*an* knock-out (Mp*an*^{ko}) and Mp*an* genome-edited (Mp*an*^{ge}) lines. (A) Genomic structures in the wild-type (Tak-1) and Mp*an* knock-out (Mp*an-1*^{ko}) lines. MpAN exons are indicated by black boxes. The hygromycin phosphotransferase gene (*hpt*) cassette is indicated by the gray box. (B) Genomic sequences in the Tak-1 and genome-edited lines. The amino acid (AA) sequence encoded by Mp*AN* is shown at top. The Tak-1 sequence is shown together with the PAM sequence (red) and the target sequence (blue). The genome-edited lines Mp*an-4*^{ge} and Mp*an-9*^{ge} have a 17 bp insertion and 214 bp deletion, respectively (orange). (C) Genotyping of the wild-type, Mp*an* knock-out, and genome-edited lines. The positions of the primers used to confirm knock-out and genome editing of MpAN are shown in *a*. Black and white arrowheads indicate the predicted sizes of the PCR products from the wild-type and knock-out Mp*an* genomes, respectively. The Y-chromosome-linked DNA marker rbm27 and the X-chromosome-linked DNA markers rhf73 and rbf62 were used for sexual genotyping.

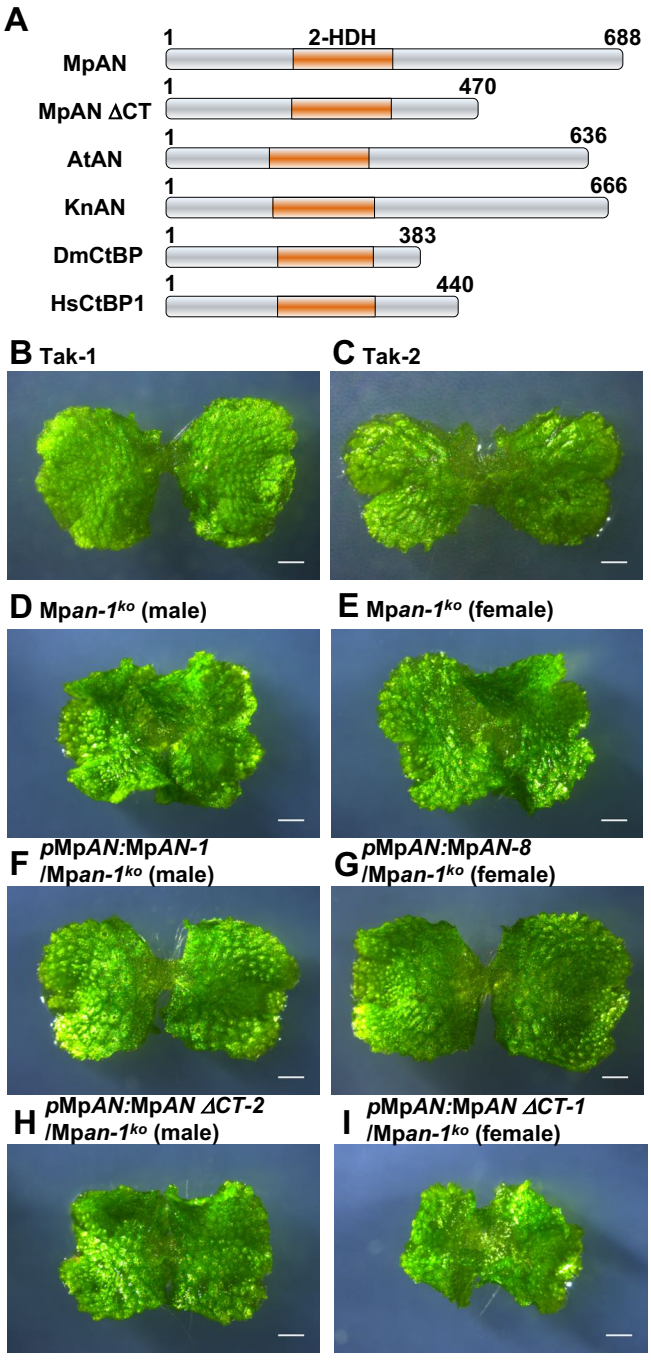

Fig. S3. Morphology of *p*Mp*AN:*Mp*AN ΔCT*/ Mp*an-1*^{ko} plants. (A) Schematic representation of plant ANs and amimal CtBPs. MpAN ΔCT is deleted for the plant specific C-terminal region. (B) Genotyping of the complementation lines. (B-I) 10-day-old gemmalings of Tak-1 (B), Tak-2 (C), Mp*an-1*^{ko} (male) (D), Mp*an-1*^{ko} (female) (E), *p*Mp*AN:*Mp*AN-1*/Mp*an-1*^{ko} (male) (F), *p*Mp*AN:*Mp*AN-8*/Mp*an-1*^{ko} (female) (G), *p*Mp*AN:*Mp*AN ΔCT-2*/Mp*an-1*^{ko} (male) (H), and *p*Mp*AN:*Mp*AN ΔCT-1*/Mp*an-1*^{ko} (female) (I). Bars, 1 mm.

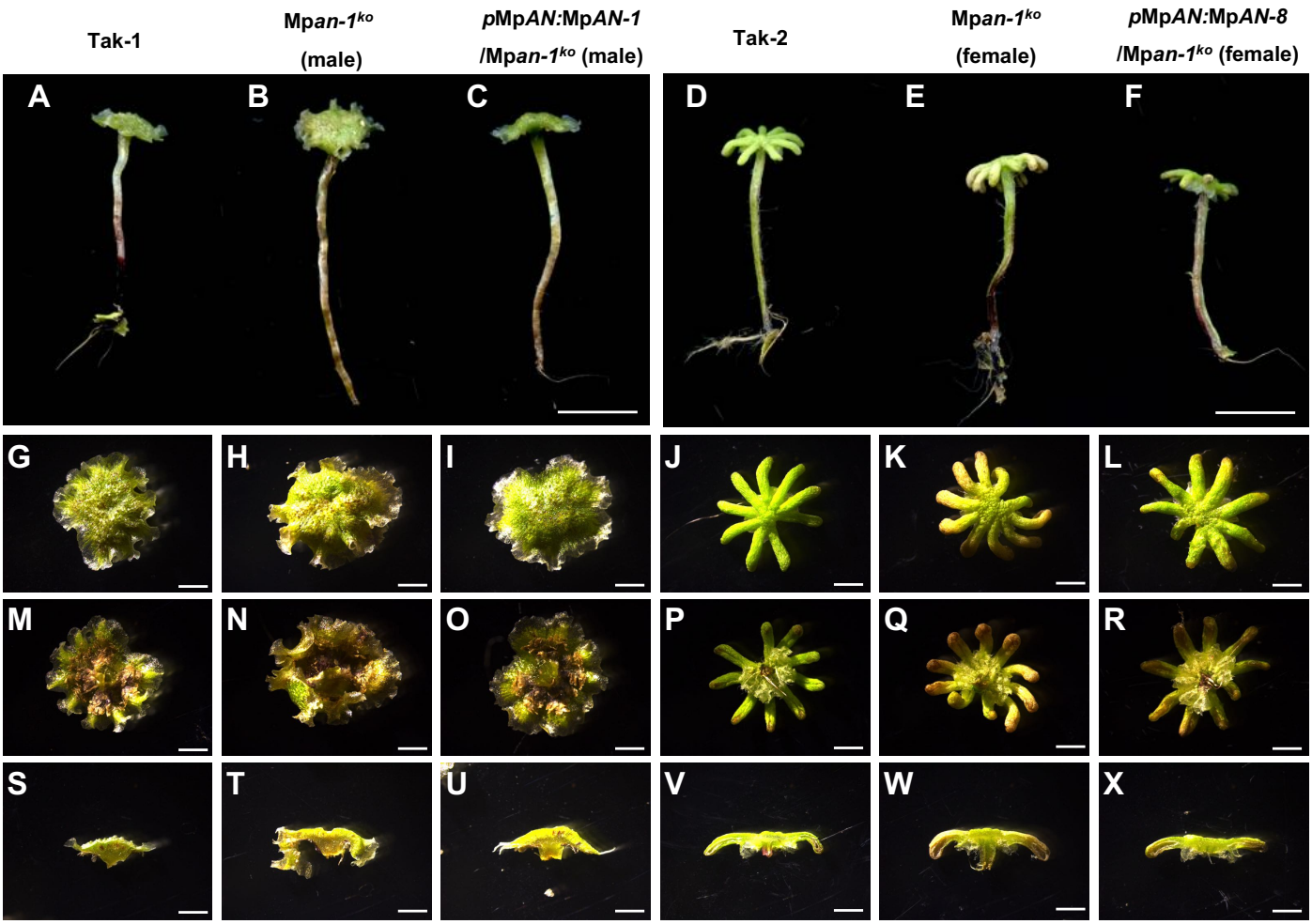

Fig. S4. Morphology of antheridiophores and archegoniophores of Mp*an* mutants. (A–F) Side views of antheridiophores of Tak-1 (A), Mp*an-1*^{ko} (male) (B), and *p*Mp*AN:*Mp*AN-1*/Mp*an-1*^{ko} (male) (C) and archegoniophores of Tak-2 (D), Mp*an-1*^{ko} (female) (E), and *p*Mp*AN:*Mp*AN-8*/Mp*an-1*^{ko} (female) (F). Bars, 1 cm. (G–R) Dorsal (G–L) and ventral (M–R) side views of antheridiophores of Tak-1 (G,M), Mp*an-1*^{ko} (male) (H,N), and pMpAN:MpAN-1/Mp*an-1*^{ko} (male) (I,O) and archegoniophores of Tak-2 (J,P), Mp*an-1*^{ko} (female) (K,Q), and pMpAN:MpAN-8/Mp*an-1*^{ko} (female) (L,R). Bars, 3 mm. (S–X) Free-hand vertical section views of antheridiophores of Tak-1 (S), Mp*an-1*^{ko} (male) (T), and *p*Mp*AN:*Mp*AN-1*/Mp*an-1*^{ko} (male) (U) and archegoniophores of Tak-2 (V), Mp*an-1*^{ko} (female) (W), and *p*Mp*AN:*Mp*AN-8/Mpan-1*^{ko} (female) (X). Bars, 3 mm.

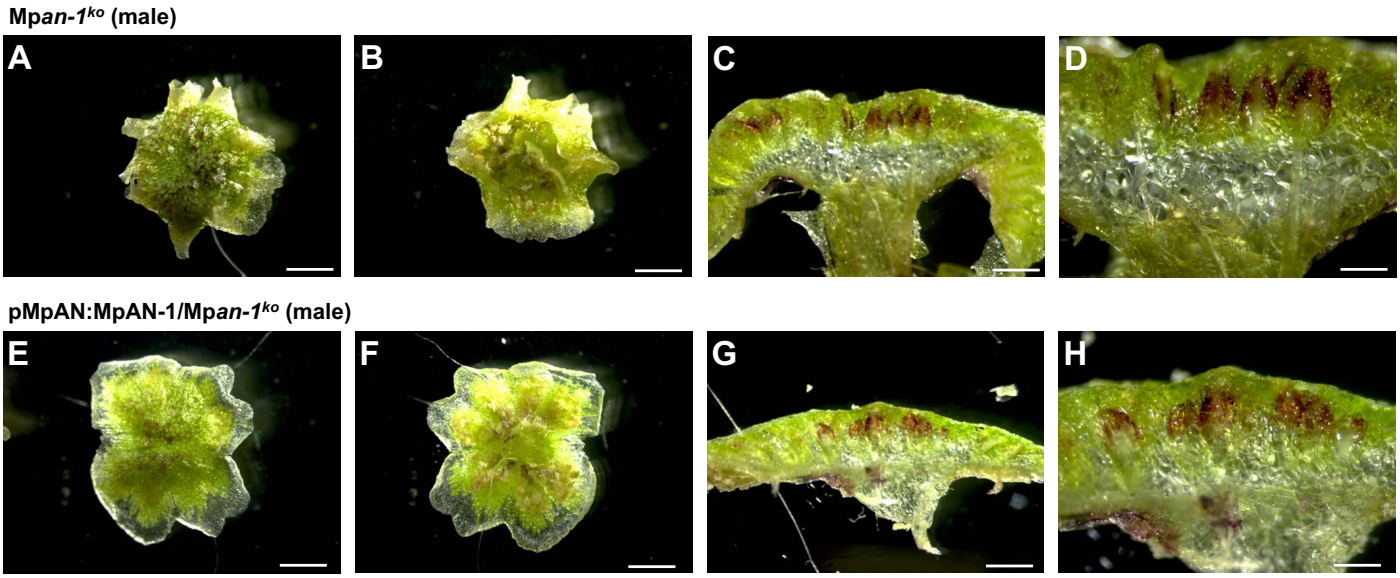

Fig. S5. Morphology of antheridiophores of Mp*an* mutants. (A–H) Antheridiophores of Mp*an-1*^{ko} (male) (A–D) and *p*Mp*AN:*Mp*AN-1*/Mp*an-1*^{ko} (male) (E–H). Dorsal (A, E), ventral (B, F), and free-hand vertical section (C, D, G, H) views. Bars, 3 mm (A, B, E, F), 0.8 mm (C, G), and 0.4 mm (D, H).

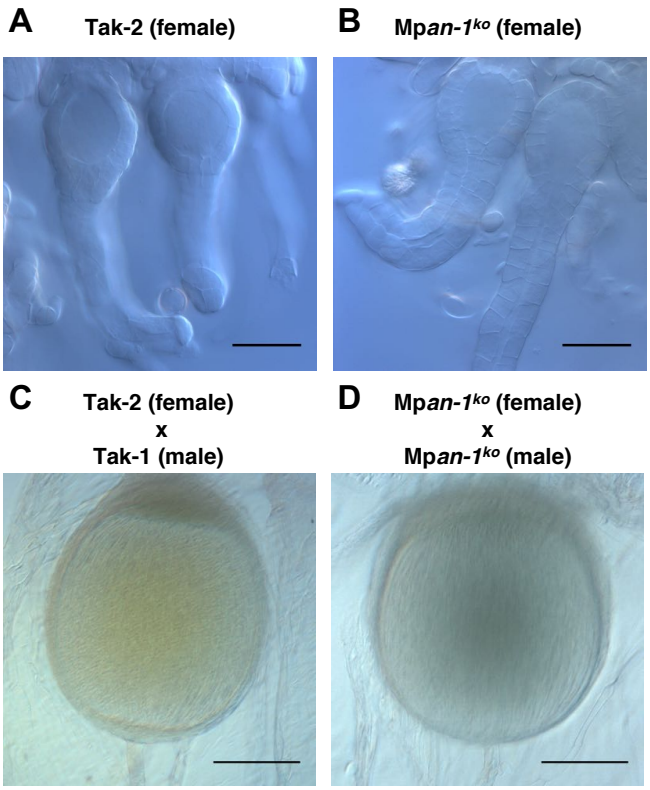

Fig. S6. Morphology of archegonniums and sporophytes of Mp*an* mutants. Archegoniums of Tak-2 (A) and Mp*an-1*^{ko} (female) (B). Sporophytes of Tak-2 with Tak-1 (C) and of Mp*an-1*^{ko} (female) with Mp*an-1*^{ko} (male) (D). Bars, 50 µm (A, B), and 200 µm (C, D).

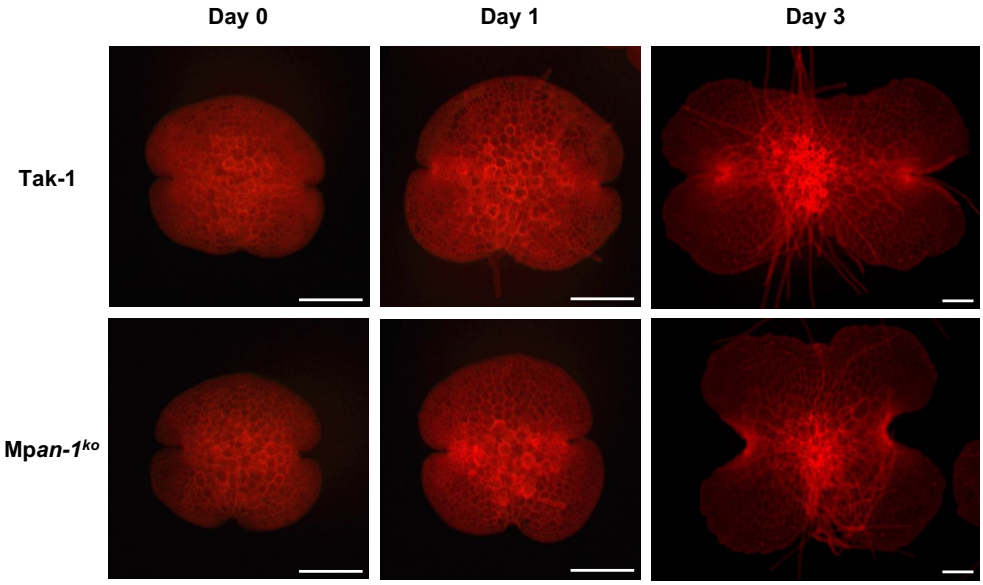

Fig. S7. Shapes of the gemmae and thalli of Mp*an* mutants. Shapes of the gemmae and thalli of Tak-1 and Mp*an-1*^{ko} (male) cultured for 0, 1, or 3 days were visualized by mPS-PI staining. Cell walls stained with PI are shown in red. Bars, 200 µm.

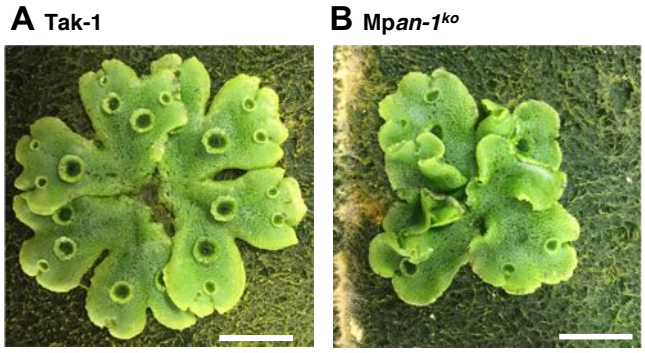

Fig. S8. Thirty-five-day-old thalli of Mp*an* mutants. (A, B) Tak-1 (A) and Mp*an-1*^{ko} (male) (B) were cultured on rockwool for 35 days. Bars, 1 cm.

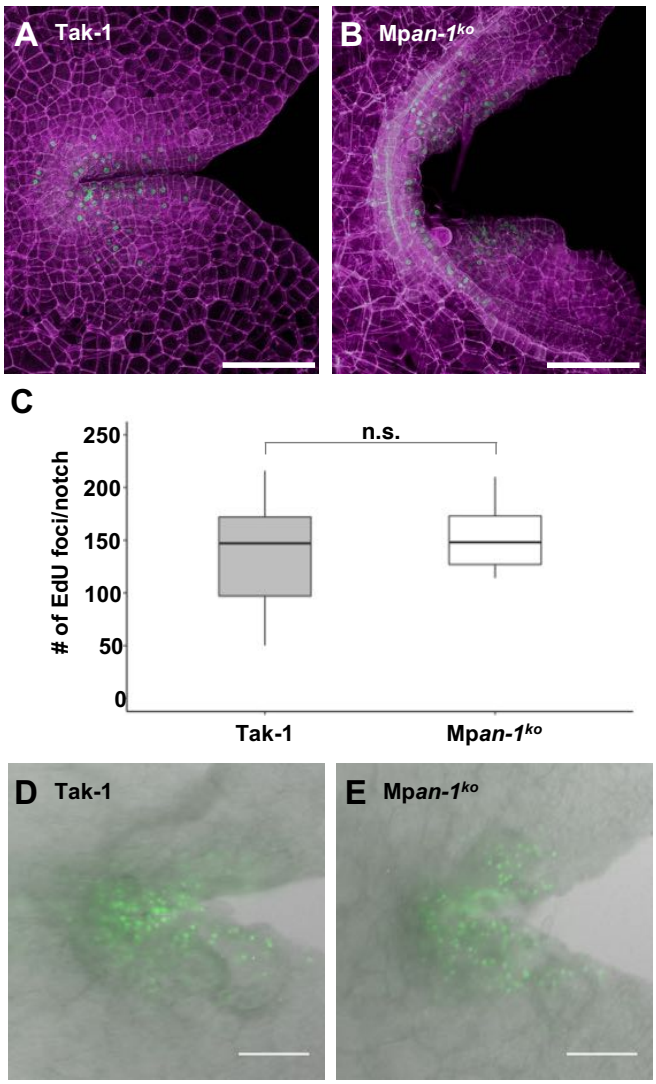

Fig. S9. Numbers of S-phase cells in Mp*an* mutants. (A, B) S-phase nuclei and cell walls in the Tak-1 and Mp*an-1*^{ko} (male) lines cultured for 3 days were visualized by EdU and mPS-PI staining, respectively. Plants were treated with EdU-containing liquid medium for 1 h. Z-series fluorescence images were obtained. Maximum projection images of Tak-1 (A) and Mp*an-1*^{ko} (male) (B) are shown. EdU-containing nuclei are shown in green and PI-stained cell walls in red. Bars, 100 µm. (C) The numbers of EdU-containing nuclei are shown in box-and-whisker plots. Number of notches, n = 13 (Tak-1) and n = 15 (Mpan-1^{ko} (male)). Asterisks indicate significant differences from Tak-1 (* $P < 0.05$, ** $P < 0.01$, Student's t-test). (D, E) S-phase nuclei in the Tak-1 and Mp*an-1*^{ko} (male) lines cultured for 5 days under weak blue light were visualized by EdU staining. Plants were treated with the EdU-containing liquid medium for 2 h. EdU-containing nuclei are shown in green overlayed with bright field image. Bars, 100 µm.

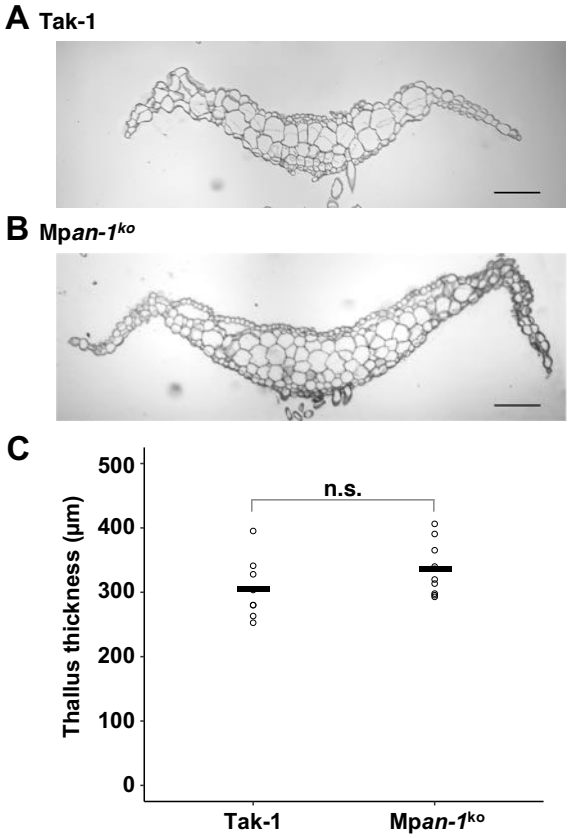

Fig. S10. Thickness of thalli in Mp*an* mutants under weak blue light. (A, B) Whole images of the transverse section of Tak-1 (A) and Mp*an-1*^{ko} (male) (B) cultured for 10 days under weak blue light. Bars, 200 µm (A, B). (C) Thicknesses of thalli are shown in violin plots. Black dots indicate values of each measurement. Black bars indicate mems of thickness values. n = 4 (Tak-1) and n = 5 (Mpan-1^{ko} (male)). Significant differences compared with Tak-1 (* $P < 0.05$, ** $P < 0.01$, Student's t-test).

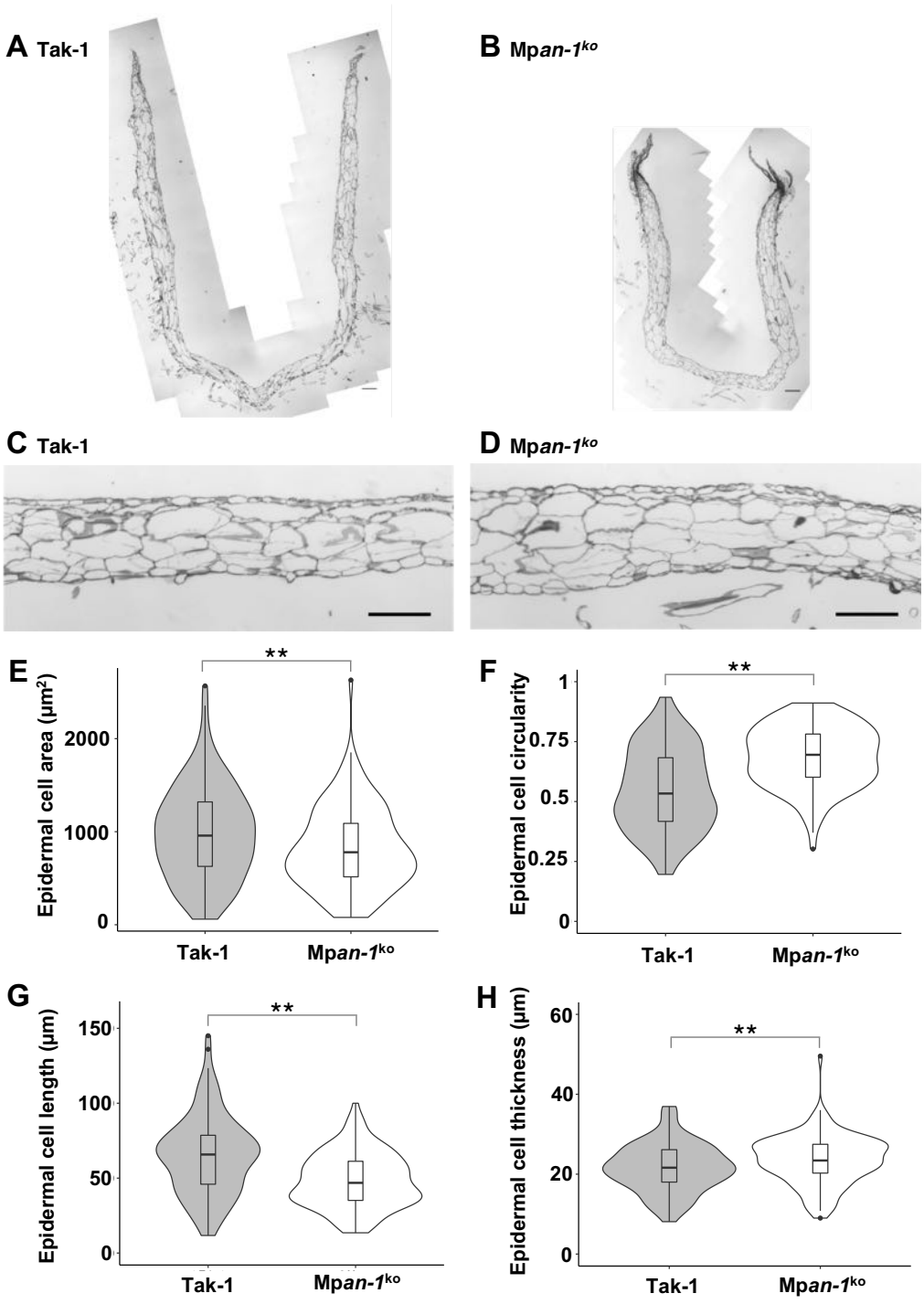

Fig. S11. Epidermal cell Morphology in Mp*an* mutants under weak blue light. (A, B, C, D) Whole images (A, B) and magnified images (C, D) of the longitudinal section of Tak-1 (A, C) and Mp*an-1*^{ko} (male) (B, D) cultured for 10 days under weak blue light. Bars, 200 μm (A, B, C, D). (E, F, G, H) Epidermal cell area (E), circularity (F), length (G), and thickness (H) are shown in violin plots with box-and-whisker plots. 108 cells from four individuals for Tak-1, and 123 cells from three individuals for Mp*an-1*^{ko} were examined. Asterisks indicate significant differences compared with Tak-1 (* $P < 0.05$, ** $P < 0.01$, Student's *t*-test).

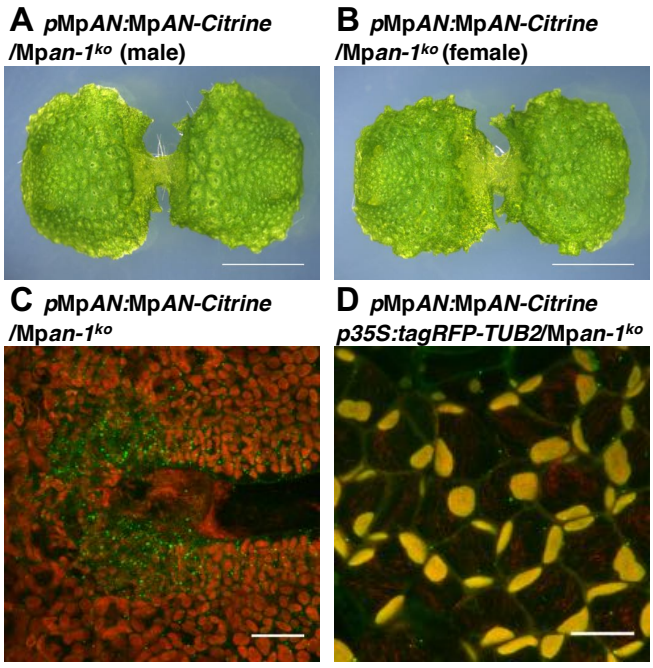

Fig. S12. Subcellular localization of MpAN-Citrine protein. (A, B) 10-day-old gemmalings of *p*Mp*AN*:Mp*AN*-Citrine/Mp*an-1*^{ko} (male) (A) and *p*Mp*AN*:Mp*AN*-Citrine/Mp*an-1*^{ko} (female) (B). Bars, 3 mm. (C) Subcellular localization of MpAN:Citrine in 2-day-old gemmalings of pMp*AN*:Mp*AN*-Citrine/Mp*an-1*^{ko} (male) transgenic plant was visualized. Citrine signals are shown in green and autofluorescence in red. (D) Subcellular localization of MpAN:Citrine and TagRFP-TUB2 in thallus of the *p*Mp*AN*:Mp*AN*-Citrine/*pCaMV35S:TagRFP-MpTUB2*/Mp*an-1*^{ko} (male) transgenic plants was visualized. Citrine signals are shown in green, TagRFP signals in red and autofluorescence in yellow. Bars, 20 µm (C, D).

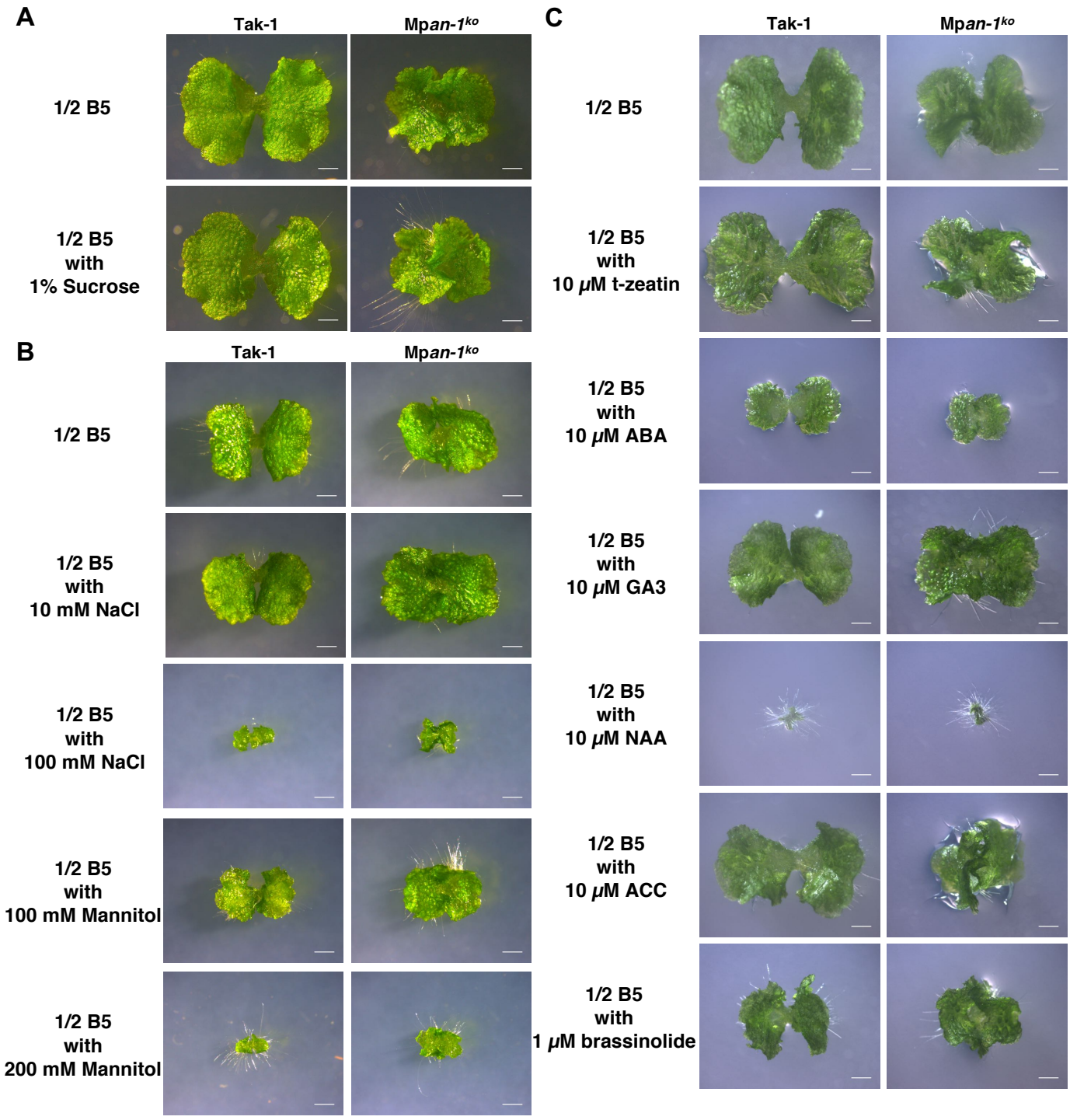

Fig. S13. Morphology of Mp*an* mutants cultured on various environmental condition and phytohormone treatments. Tak-1 and Mp*an-1*^{ko} were cultured for 10 days on each indicated culture medium to test the response to sucrose (A), salt and osmotic stresses (B), and phytohormones (C). Bars, 1 cm.

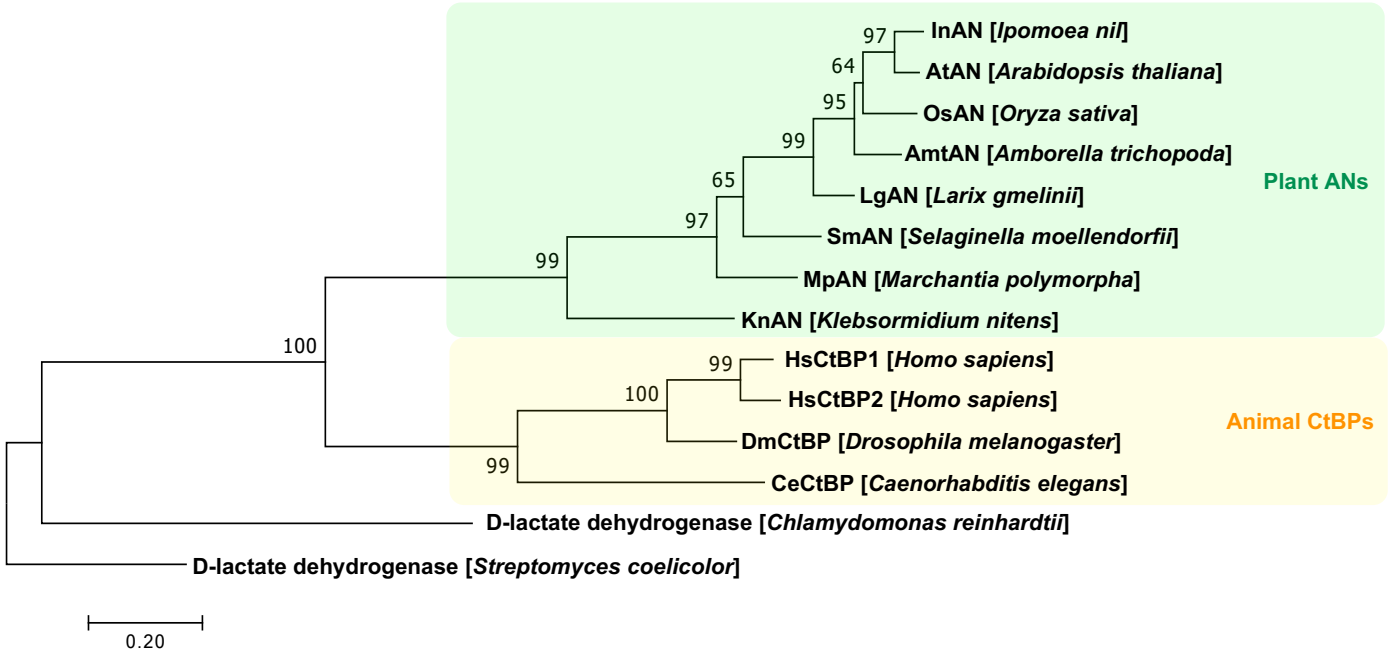

Fig. S14. Phylogenic analysis of plant ANs and animal CtBPs. Phylogenetic analysis of the amino acid sequences of plant ANs and animal CtBPs was carried out. D-lactate dehydrogenases of *C. reinhardtii* and *Streptomyces coelicolor* were evaluated. The amino acid sequences of the D2-HDH motifs were aligned using CLUSTALW, and a phylogenic tree was drawn using the maximum-likelihood method with bootstrapping of 1,000 replicates.

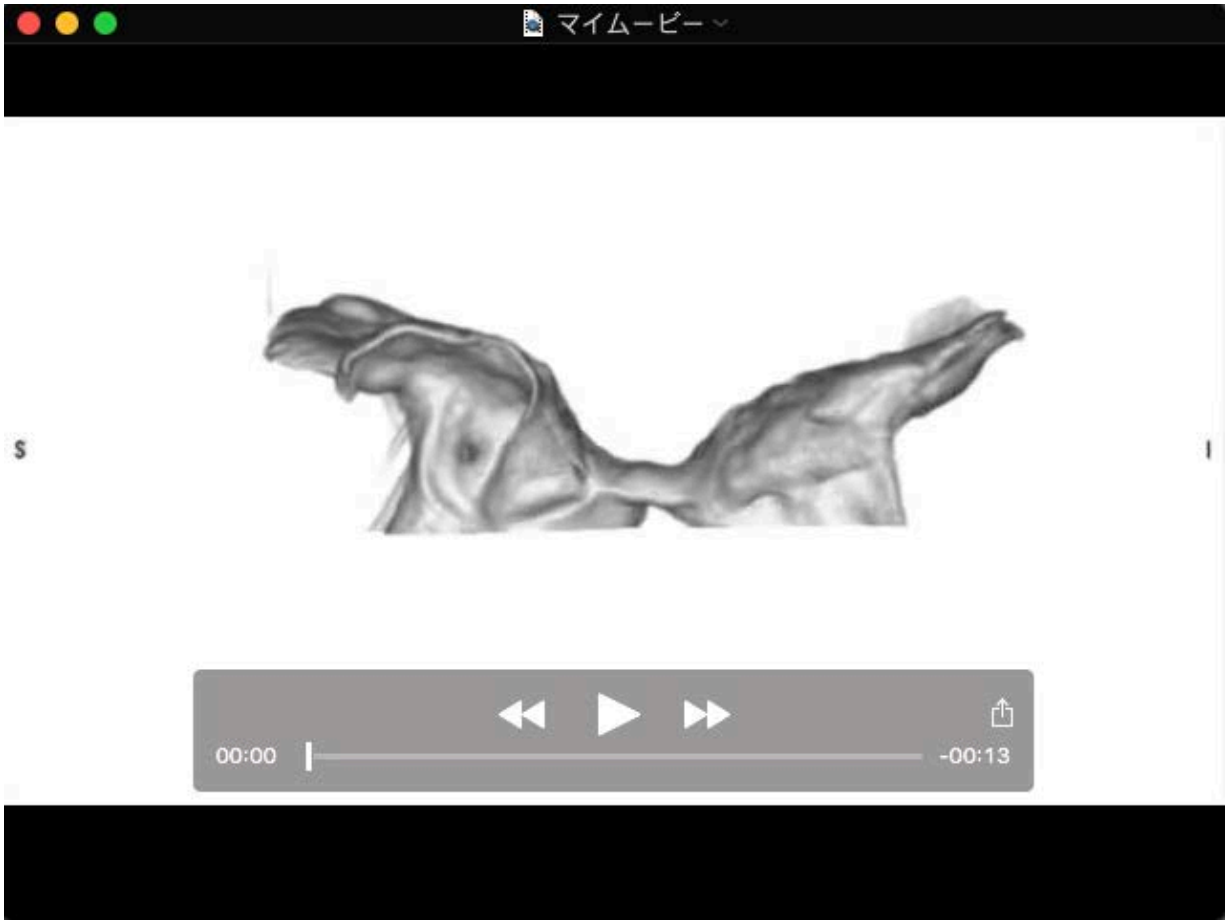

Movie S1. Micro-CT image of a wild-type gemmaling. Micro-CT image of a 10-day-old gemmaling of Tak-1.

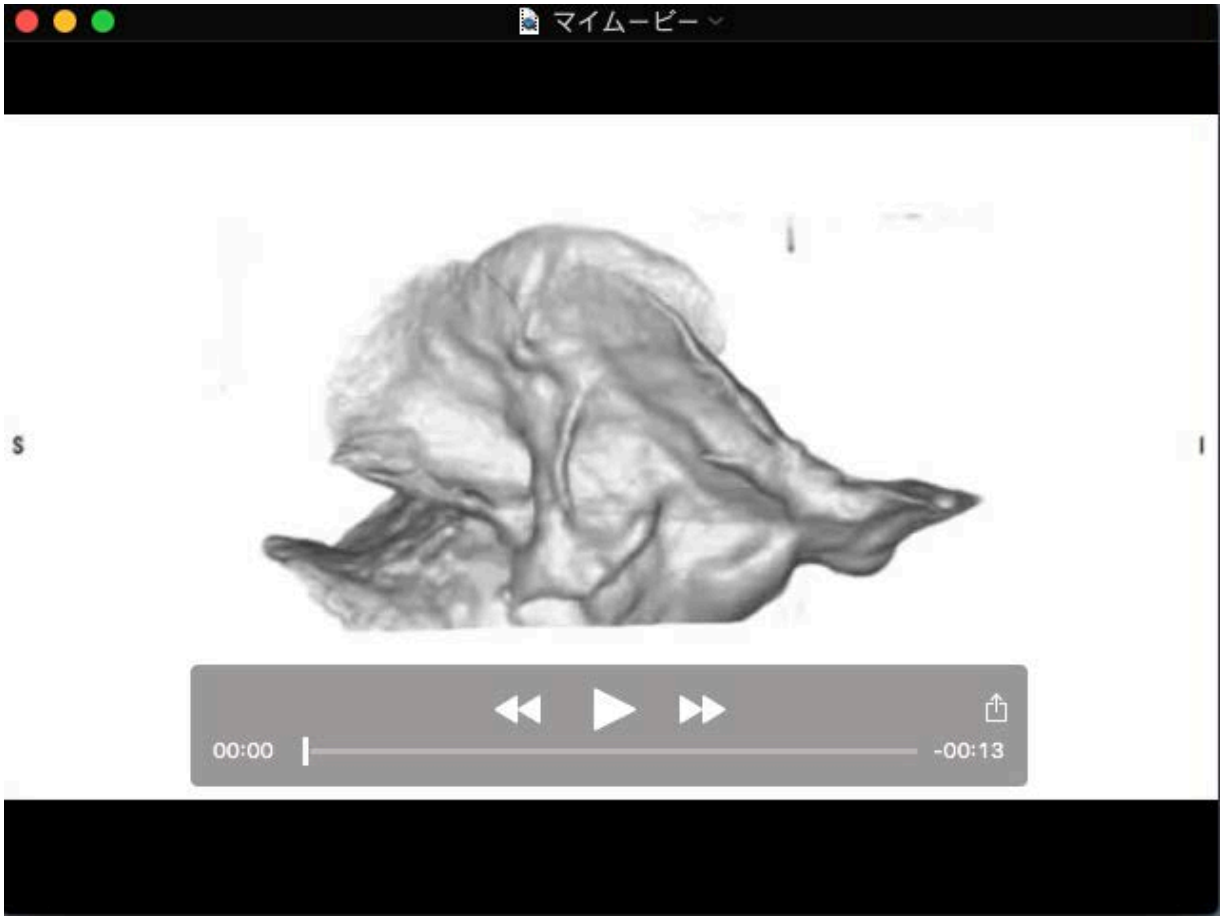

Movie S2. Micro-CT image of an Mp*an* knock-out mutant gemmaling. Micro-CT image of a 10-day-old gemmaling of Mp*an-1*^{ko} (male).